Song, Wei Jie

THEORETICAL MODELING OF PERIPHERAL TISSUE AND WHOLE LIMB HEAT-TRANSFER

City University of New York PH.D. 1987

THEORETICAL MODELING OF PERIPHERAL TISSUE AND WHOLE LIMB HEAT TRANSFER

by

WEI JIE SONG

A dissertation submitted to the Graduate Faculty in Engineering in partial fulfillment of the requirements for the degree of Doctor of Philosophy, The City University of New York.

1987

This manuscript has been read and accepted for the Graduate Faculty in Engineering in satisfaction of the dissertation requirement for the degree of Doctor of Philosophy.

4/29/87

Date

Sheldon Weinbaum

CUNY Distinguished Professor

Sheldon Weinbaum (Mentor)

Chair of Examining Committee

4/29/87

Date

Paul R. Karmel

Professor Paul R. Karmel

Executive Officer

Dean Charles Watkins

H. Kayser Professor Latif M. Jiji (Co-mentor)

Doctor Daniel E. Lemons

Professor Zeev Dagan

Professor Shu Chien

Supervisory Committee

The City University of New York

Abstract

THEORETICAL MODELING OF PERIPHERAL TISSUE
AND WHOLE LIMB HEAT TRANSFER

by

Wei Jie Song

Adviser: Professor Sheldon Weinbaum
Professor Latif M. Jiji

In the first part of this dissertation the new bioheat equation derived in Weinbaum and Jiji [10] is applied to a three layer conceptual model of microvascular surface tissue organization. A simplified one-dimensional quantitative model of peripheral tissue energy exchange is then developed. A representative vasculature is constructed for each layer and the enhancement in the local tensor conductivity of the tissue as a function of vascular geometry and blood flow is examined. Numerical solutions for the boundary value problem coupling the three layers are presented and these results used to study the thermal behavior of peripheral tissue for a wide variety of physiological conditions from supine resting state to maximum exercise.

In the second part a new basic model for whole limb heat transfer is proposed wherein the countercurrent heat from the large central artery and vein is coupled to the microvascular heat exchange in the surrounding muscle tissue and the outer cutaneous layer by matching the far field conduction solution from the central vessels to the local microvascular

temperature field in the muscle tissue described by the new bioheat equation of Weinbaum and Jiji. This fundamental coupling shows how large primarily unequilibrated vessels can be integrated within the temperature field of a perfused tissue whose thermally significant microvessels are close to equilibrium with the local mean tissue temperature. The new model allows for an arbitrary axial variation of cross-sectional area and blood distribution between the muscle and cutaneous tissue, includes the heat transfer at the skin surface, accounts for the blood flow to and heat loss from the extremity and treats the venous return temperature and surface temperature distribution as unknowns that are determined as part of the solution to the overall boundary value problem. Representative solutions are also presented for a wide range of environmental conditions for the limb in both the resting state and during exercise.

ACKNOWLEDGEMENTS

I wish to thank Professor Sheldon Weinbaum and Professor Latif M. Jiji for their support and valuable guidance during the course of this research. I also wish to thank Doctor Daniel E. Lemons and Professor Zeev Dagan for their encouragement and helpful and illuminating discussions.

I am grateful to Professor Paul R. Karmel for handling administrative details in such a warm and friendly manner.

This research was supported by Grant No. 5 R01 HL 26090 from the National Institutes of Health.

CONTENTS

LIST OF SYMBOLS

a	vessel radius of muscle layer
a_a	radius of artery; radius of central artery in Chap.3
a_{ai}	radius of central artery at entrance of limb
a_v	radius of vein; radius of central vein in Chap.3
a_b	vessel radius at base of deep tissue layer in Chap.2; vessel radius of muscle layer at interface between core and muscle in Chap.3
B_{ic}	convective Biot number = $h_c r_{si} / K_t$
B_{ir}	radiative Biot number = $h_r r_{si} / K_t$
c	specific heat of tissue
c_b	specific heat of blood
e	spacing between centers of countercurrent vessel pair
e_a	distance between center of artery and origin in Fig.11
e_v	distance between center of vein and origin in Fig.11
G	dimensionless shape function representing axial variation of arm geometry
g	blood bleed-off per unit vessel surface area
g_a	blood bleed-off from artery per unit vessel surface area
g_v	blood bleed-off to vein per unit vessel surface area
h_c	convective heat transfer coefficient
h_r	radiative heat transfer coefficient
K	conductivity
K_b	blood conductivity
$(K_{ij})_{eff}$	tensor of effective conductivity
K_{eff}	effective conductivity

K_t tissue conductivity

L length of arm

L_e thermal equilibration length of vessel

L_n thickness of n th layer

ℓ_i , ℓ_j directional cosine of vessel axis with respect to direction i (or j) where i=1 is direction perpendicular to skin surface

ℓ_r directional cosine of vessel axis with respect to radial direction

M_a shape factor = e_a/a_a

M_v shape factor = e_v/a_v

n number density of vessel pairs of muscle layer

n_o number density of vessel pairs at base of deep tissue layer in Chap.2; number density of vessel pairs of muscle layer at interface between core and muscle in Chap.3

P_e local Peclet number = $2\rho_b c_b a u/K_b$

P_{ei} inflow Peclet number at entrance of limb = $2\rho_b c_b a_{ai} u_{ai}/K_b$

P_{eo} inflow Peclet number at base of deep tissue layer = $2\rho_b c_b a_o u_o/K_b$

P_m blood bleed-off rate to muscle layer per unit length of central artery

P_s blood bleed-off rate to cutaneous layer per unit length of central artery

Q_c volumetric blood flow rate into cutaneous layer per unit area

Q_{DI} volumetric blood flow rate into deep and intermediate layers per unit area

q rate of energy transfer by conduction between countercurrent vessel pair per unit length of vessel

q_a rate of energy transfer by conduction at artery wall per unit length of artery

q_{ev} rate of energy transfer by evaporation per unit area of skin surface

q_{ext} total heat transfer rate on extremity surface

q_m metabolic heat production of muscle layer

q_n distributed heat source in n th layer (due to blood perfusion or metabolism)

q_v rate of energy transfer by conduction at vein wall per unit length of vein

q/A heat flux

$(q/A)_c$ convective heat flux on skin surface

$(q/A)_r$ radiative heat flux on skin surface

R ratio of cutaneous layer blood supply to combined deep tissue and intermediate layers blood supply $= Q_c/Q_{DI}$

r coordinate in radial direction

r_c radius of core

r_{ci} radius of core at entrance of limb

r_s radius of surface

r_{si} radius of surface at entrance of limb

$\tilde{r}$ dimensionless coordinate in radial direction $= r/r_{si}$

$\tilde{r}_c$ dimensionless radius of core $= r_c/r_{si}$

$\tilde{r}_s$ dimensionless radius of surface $= r_s/r_{si}$

S_{DI} length of countercurrent vessel pair from its entrance at base of deep tissue layer

s coordinate along vessel axis

T tissue temperature

T_a blood temperature of artery; blood temperature of central artery in Chap.3

T_{ai} blood temperature of central artery at entrance of limb

T_s surface temperature

T_v blood temperature of vein; blood temperature of central vein in Chap.3

T_{vi} blood temperature of central vein at entrance of limb

T_o local arterial supply temperature

T_{oo} tissue temperature at origin in Fig.11

T_∞ ambient temperature

$\tilde{T}_a$ dimensionless blood temperature of central artery $= (T_a - T_\infty)/(T_{ai} - T_\infty)$

$\tilde{T}_v$ dimensionless blood temperature of central vein $= (T_v - T_\infty)/(T_{ai} - T_\infty)$

t time

u blood velocity in vessels of muscle layer

u_a blood velocity of artery; blood velocity of central artery in Chap.3

u_{ai} blood velocity of central artery at entrance of limb

u_v blood velocity of vein; blood velocity of central vein in Chap.3

u_{vi} blood velocity of central vein at entrance of limb

u_o blood velocity in vessels at base of deep tissue layer in Chap.2; blood velocity in vessels at interface between core and muscle in Chap.3

V blood perfusion rate per unit volume

W_b volumetric blood perfusion rate per unit volume

W_{bc} volumetric blood perfusion rate to cutaneous layer per unit volume

x general coordinate; coordinate in axial direction in Chap.3

x_i , x_j general coordinate

$\tilde{x}$ dimensionless coordinate in axial direction = x/L

y	general coordinate
z	general coordinate
z_n	coordinate in n th layer
$\tilde{z}$	dimensionless general coordinate
$\tilde{z}_n$	dimensionless coordinate in n th layer = z_n/L_n
α	length defined by Eq.(43)
β	shape factor defined by Eq.(56)
γ	dimensionless evaporation heat loss = $q_{ev} r_{si} / K_t (T_{ai} - T_\infty)$
δ_{ij}	Kroneker delta
δ_1	thickness of inner region of cutaneous layer of arm
δ_2	thickness of outer region of cutaneous layer of arm
ϵ	emissivity of skin
θ	tissue temperature
θ_{bc}	temperature of blood entering cutaneous plexus
θ_n	tissue temperature in n th layer
$\tilde{\theta}$	dimensionless tissue temperature in Chap.3 = $(\theta - T_\infty)/(T_{ai} - T_\infty)$
$\tilde{\theta}_{bc}$	dimensionless temperature of blood entering cutaneous plexus = $(\theta_{bc} - T_s)/(T_0 - T_s)$ in Chap.2; = $(\theta_{bc} - T_\infty)/(T_{ai} - T_\infty)$ in Chap.3
$\tilde{\theta}_n$	dimensionless tissue temperature in n th layer = $(\theta_n - T_s)/(T_0 - T_s)$
λ_m	dimensionless metabolic heat production of muscle layer = $q_m r_{si}^2 / K_t (T_{ai} - T_\infty)$
λ_n	dimensionless distributed heat source in n th layer = $q_n L_n^2 / K_t (T_0 - T_s)$
ρ	density of tissue
ρ_b	density of blood
$\overline{\rho c}$	average blood-tissue heat capacity per unit volume

σ shape factor of vessels of muscle layer; Stefan-Boltzmann constant

σ_c shape factor of central artery-vein pair defined by Eq.(53)

ψ blood supply to arm / blood supply to whole limb

ω blood supply to muscle layer / blood supply to arm

Subscripts:

n = 1,2,3,4 corresponding to deep tissue layer, intermediate layer, inner and outer regions of cutaneous layer. See Fig.5

LIST OF TABLES

LIST OF FIGURES

1. Introduction

1.1 Background

Homeotherms are animals, including man, who continuously exchange heat with their environment, and yet maintain the body temperature over a narrow range of less than a degree, in spite of widely varying environmental conditions and levels of activity. The maintenance of a constant internal temperature is an important requirement for the establishment and support of life for these beings. The basis of this requirement is the profound effect of temperature on the structure and interaction of biomolecules, which in turn regulate biological function. Thus it is not surprising that a study of the response of homeotherms to environmental and internal thermal stresses occupies an important position in the life sciences. More than a billion dollars is spent annually on the design of space suits, diving equipment, incubators and other local environments and in medical applications involving hyperthermia applicators, cryosurgical probes, thermal blood flow sensors and thermographic tumor detection equipment to mention a few of the more common applications. Truly reliable physiologically based models of biological heat transfer would not only be invaluable in the design of these devices, but also play a crucial role in quantitatively interpreting the numerous physiological measurements that have been obtained to elucidate the intricate thermal functioning of the human body.

The heat transfer function of the vascular system of the living body has been appreciated since the mid-19th century

and the local tissue heat transfer quantitatively modeled since the work of Pennes (1948) [1]. The bioheat equation proposed by Pennes, which is

$$\bar{\rho c}\frac{\partial T}{\partial t} = \nabla\cdot K\nabla T + W_b\rho_b c_b(T_a - T) + q_m \qquad (1)$$

has formed the basis of most theoretical studies in bioheat transfer over the past three decades. This equation has been used in a wide diversity of applications including limb and whole body heat transfer models. Some of the applications are summarized in a recent two volume authoritative review edited by Shitzer and Eberhart [2] describing the state of the art in bioheat transfer.

The crucial term in the Pennes bioheat equation is the blood perfusion term which describes the local heat transfer between blood and tissue. In the Pennes equation this term is treated as a volumetric, isotropic heat source which derives from the commonly held view that heat exchage, like gas, water and solute transport, occurs primarily in the capillary beds and the small arterioles and venules that feed them due to their very large surface area for exchange compared to the larger microvessels. According to this view arterial blood at the local arterial supply temperature would be delivered to the capillaries where thermal equilibration to the local tissue temperature would occur. While several investigators have questioned the isotropic assumption [3,4], the pioneering paper by Chen and Holmes [5] showed that because the thermal conductivity coefficient is typically three orders of magnitude larger than the gaseous diffusion coefficient,

thermal equilibration could not possibly occur in single vessels which these authors theoretically estimated to be less than 50 μm. Subsequent simplified models of other basic geometries with constant area vessels Chato [6] and Weinbaum et al. [7] showed that countercurrent exchange was particularly efficient in vessels over 50 μm and appeared to dominate the conduction loss to the neighboring tissue in these vessels.

The paper by Weinbaum, Jiji and Lemons [7] was a turning point in that it contained the first pilot experiments in which temperature measurements were made in the vicinity of thermally significant microvessels which were subsequently correlated by vascular casting techniques with particular vascular elements. Substantial temperature differences between blood and tissue in the larger microvessels could not be found suggesting that even in these larger vessels thermal equilibration was occuring very rapidly. Equally important was the observation that with few exceptions all vessels over 50 μm occured as closely spaced countercurrent pairs and that the microvascular geometry of peripheral tissue varied primarily with depth from the skin surface. An elaborate mathematical model of a continuously branching microvascular network was then developed in Jiji et al. [8] to explain this unusual behavior. Parametric studies by Dagan et al. using this detailed model [9] showed that the vessels over 50 μm functioned almost but not exactly as a perfect countercurrent heat exchanger and that the mean axial temperature of the

artery-vein pair would have to follow the mean tissue temperature gradient if a large divergence in temperature between blood and tissue was to be avoided. This model traced the local blood-tissue temperature difference all the way to the capillary beds and predicted that the blood perfusion source term in the Pennes equation was zero. It has become increasingly evident from these studies that the specialized microvascular organization of peripheral tissue serves a vital physiological function in living body heat transfer. Vascular casts of peripheral tissue show that the skeletal muscle tissue just beneath the very thin cutaneous layer is comprised largely of separated small transverse vessels under 50 μm diameter and their capillary beds. If thermal equilibration was to occur in these small microvessels, as assumed in Pennes equation, large energy losses from the body to the surroundings would occur in a cold environment and the body would have great difficulty maintaining thermal homeostasis!

A fundamental new bioheat equation was derived in Weinbaum et al. [10] to replace the Pennes equation and describe this new microvascular heat exchange mechanism which was termed incomplete countercurrent heat exchange. This derivation assumed that the paired vessels could be treated locally as having an equal and opposite mass flow and that the local temperature field surrounding the vessels was given by the local conduction solution in the cross-sectional plane. It was further assumed that the far field temperature obtained from this solution was to lowest order the local

average temperature of the tissue. In the new bioheat equation the effective conductivity of the tissue is related to the local vascular geometry and flow of the vessel pairs.

Starting with a differential control volume shown in Figure 1, one can show from conservation of mass and energy applied to both the tissue and thermally significant countercurrent vessels that the standard heat conduction equation must be modified to

$$\bar{\rho}c\frac{\partial\theta}{\partial t} - \nabla\cdot K\nabla\theta = n(q_a - q_v) + 2\pi\rho_b c_b n a_a g_a (T_a - T_v) + q_m \qquad (2)$$

where

$$q_a - q_v = -\pi\rho_b c_b a_a^2 u_a \frac{d(T_a - T_v)}{ds} \qquad (3)$$

to describe the effect of blood flow. θ here represents a local average tissue temperature, whose definition is subtle and will be discussed shortly, and $T_a - T_v$ is the local arterial-venous temperature difference. The first term on the right hand side of equation (2) describes the net conduction loss per unit volume from n vessel pairs/cm^2 to the tissue and the second term the energy loss due to the small vessel bleed-off from the countercurrent artery to vein.

A critical part of the analysis is the development of a closure hypothesis to relate $T_a - T_v$ to the local average tissue temperature θ. In the original formulation [10] θ was simply taken as the mean of T_a and T_v or the far field temperature that would result if the vessels were of equal size and a local conduction solution assumed to apply in the plane perpendicular to the vessel axis. A detailed

experimental confirmation of the theory has recently been completed by Lemons et al. [11] and has shown that the basic conduction nature of the thermal field in the vicinity of the vessels of unequal size is correct, but that refinements were necessary for the proper definition of θ. The closure hypothesis in [10] led to the following relationship for the local arterial-venous temperature difference,

$$\pi \rho_b c_b a_a^2 u_a \frac{d\theta}{ds} = -\sigma K_t (T_a - T_v) \qquad (4)$$

where the symbols have their usual meaning and σ is a shape factor depending on the vessel radii and their local spacing. Equation (2), using results (3) and (4), can be rewritten after algebraic manipulation in the tensor form

$$\overline{\rho c} \frac{\partial \theta}{\partial t} - \frac{\partial}{\partial x_i}\left[(K_{ij})_{eff} \frac{\partial \theta}{\partial x_j}\right] = -\frac{\pi^2 n a_a^2 K_b^2}{4\sigma K_t} P_e^2 \ell_j \frac{\partial \ell_i}{\partial x_j} \frac{\partial \theta}{\partial x_j} + q_m \qquad (5)$$

where the effective tissue conductivity due to the blood flow and bleed-off from the countercurrent vessels is given by

$$(K_{ij})_{eff} = K_t \left(\delta_{ij} + \frac{\pi^2 n a_a^2 K_b^2}{4\sigma K_t^2} P_e^2 \ell_i \ell_j\right) \qquad (6)$$

Here P_e is the local Peclet number and ℓ_i, ℓ_j are the directional cosines of the vessel axes measured relative to the coordinate directions. The effective conductivity is a tensor since the vessel axes can have an arbitrary direction relative to the tissue temperature gradient. The first term on the right hand side of (5) is due to the curvature (changing direction) of the vessels.

Equation (4) has a very simple physical interpretation related to the Prandtl mixing length which is easily illustrated by the one-dimensional flow geometry in Figure 2

where the vessel axes and the tissue teperature gradient are both in the x-direction. In this sketch there is no net mass flow crossing the plane x, since the flow in the artery and vein are the same, yet there is a convective energy flux crossing this plane if there is a thermal gradient in the flow direction. Since the artery and vein cross the plane x from opposite directions and retain the memory of the tissue temperature on each side of this plane because of their finite thermal relaxation length, the arterial and venous blood at plane x have slightly different temperatures. For convenience let us assume that the thermal equilibration length L_e is the same for both artery and vein. Since the far field temperature of the vessels must match the tissue temperature, the temperature gradient along each vessel must to lowest order equal the tissue temperature gradient in the far field. Therefore the temperatures of arterial and venous blood crossing x is given by

$$T_a(x) = \theta(x) - \frac{\partial \theta}{\partial x} L_e \qquad (7)$$

and

$$T_v(x) = \theta(x) + \frac{\partial \theta}{\partial x} L_e \qquad (8)$$

Subtracting equation (8) from (7) and comparing the result with (4) one observes that L_e is $\pi a_a K_b \rho_e / 4\sigma K_t$. The sum of the conductive and convective energy flux crossing plane x is

$$q/A = -K_t \frac{\partial \theta}{\partial x} + n\pi \rho_b c_b a_a^2 u_a (T_a - T_v) \qquad (9)$$

When equations (7) and (8) are applied, (9) can be rewitten

as

$$q/A = -K_t(1 + 4n\sigma L_e^2)\frac{\partial \theta}{\partial x} \qquad (10)$$

The term $K_t(1+4n\sigma L_e^2)$ is the effective thermal conductivity and the second term in parentheses is the enhancement due to the countercurrent heat exchange. In the three-dimensional case, the effective conductivity becomes

$$(K_{ij})_{eff} = K_t(\delta_{ij} + 4n\sigma L_e^2 \ell_i \ell_j) \qquad (11)$$

Note that equations (6) and (11) are actually identical. In turbulent flow the mechanism which gives rise to a Reynolds stress and a term in the Navier-Stokes equation which has the same appearance as the molecular diffusive stress is due to finite length convective eddies. The finite thermal relaxation length here plays the same role for a countercurrent vessel pair (note an isolated vessel would produce a convective energy term since there would be a net mass transfer) and it is therefore not surprising that countercurrent convection produces an effective conductivity (6) which has exactly the same appearance as the usual molecular diffusion term in (5) and there is no convection term.

1.2 Experimental Verification of New Bioheat Equation

There are two crucial assumptions in the derivation of the new bioheat equation. The first is that the temperature gradients along the axes of the countercurrent artery and vein follow with only small deviations the local average tissue temperature gradient in the far field of the vessel pair. The second is that the local two-dimensional temperature

field in planes perpendicular to the vessel axes is to lowest order a conduction field that is negligibly affected by the small vessel bleed-off and perfusion in the vicinity of the countercurrent vessels. If these two assumptions are true the far field or local average tissue temperature will be the same as the integrated average temperature obtained from the local conduction solution in the cross-sectional plane. If there were no net heat loss from the countercurrent vessel pair (perfect countercurrent heat exchanger), the artery, vein and tissue temperature gradients would have to be identical for the far field of the inner solution to match the near field of the outer solution for the local tissue temperature.

A rigorous experimental verification of these two basic assumptions has just been completed by Lemons et al. [11]. Detailed thermal traverses were analyzed in proximity to 137 vascular elements taken from all regions of the rabbit thigh. The precise trajectory of the thermocouple wire was established by using a tissue clearing technique in which the wire was left in place after the animal was sacrificed so that its relationship to vascular elements could be ascertained when the tissue was made translucent by treatment with glycerin and examined in serial sections after the vessels were made opaque by injecting silicone elastomer. A representative traverse in close proximity to a counter-current vessel pair is shown in the right panel of Figure 3 where temperature measurements were taken at 20-40 μm

intervals as the wire was drawn through by the microdrive system. Output data were Fourier transformed to produce a smooth mean tissue temperature curve and the temperature excursions measured relative to this smooth curve. An approximate theory was then developed to determine the average blood temperature in the vascular element from measurements of the local temperature field in the vicinity of the vessels. The results showed that even when temperature gradients approaching $10^{\circ}C/cm$ were established in the tissue the temperature in the vessels would follow the tissue temperature to within less than $0.2^{\circ}C$ for all countercurrent microvessels. These measurements clearly established the validity of the first assumption.

The second assumption is critical in analyzing the local temperature field in the vicinity of the vessel pair. Based on the arguments given previously one would not expect the directed small vessel bleed-off to effect the conduction field near the vessels since the theory in [7] predicts that the thermal equilibration of these small vessels should occur over a distance of less than one diameter. This prediction is strongly supported by the close agreement of the temperature profiles in panels A and B of Figure 3. The in vivo temperature field associated with the fine wire traverse shown in panel B was simulated by a larger scale laboratory model for a countercurrent heat exchanger in which the Peclet number was approximately reproduced. The difference between the theoretical and experimental curves for the model is due

to the angular variation of the wall temperature in the laboratory experiment, which is hard to approximate in a simple theoretical model.

The most surprising new result of these detailed experiments was that the countercurrent arteries produced three times as many positive thermal signatures as the countercurrent veins and that arteries with dimensions of as small as 100 μm could be detected (temperature excursion more than two standard deviations from the mean) whereas veins had to be larger than 300 μm to be detected by this same criterion. These observations were obviously incompatible with the approximation used in the original derivation of equation (5) in which it was assumed that the local average tissue temperature was the mean of the artery and vein temperatures. An analysis of the conduction field in the cross-sectional plane in Zhu et al. [12] showed that this unexpected behavior could be accounted for if new expressions for the far field or local average tissue temperature were used in the analysis of the data which took into account the significant difference in size between the countercurrent artery and vein. In [12] the form of the new bioheat equation and effective conductivity, equations (5) and (6), are unaltered, but the shape factor σ must be changed to describe the unequal radii of the vessels. The experimental confirmation of the new bioheat equation and its refinement now appear complete. These developments have set the stage for a new generation of bioheat transfer models and quantitative

interpretation of a host of new thermophysiological measurements.

In summary, the bioheat equation of Weinbaum and Jiji (5) differs from the Pennes equation (1) in two fundamental respects: (i) the thermal source term in (1) due to small vessel perfusion does not appear at all since these vessels are already fully equilibrated and (ii) the effect of blood flow in the larger microvessels has been shown to be equivalent to a novel countercurrent mixing length behavior where the mixing length is directly related to the microstructure and flow.

In this research the new bioheat equation developed by Weinbaum and Jiji will be reduced to simplified forms for convenient use in heat transfer studies for which the bioheat equation of Pennes has been extensively used in the past. This will include (i) a new model for peripheral tissue heat transfer, (ii) a new model for heat transfer in an entire limb.

2. Simplification of Bioheat Equation of Weinbaum and Jiji and Application to Peripheral Tissue Heat Transfer

2.1 Objectives

The bioheat equation of Weinbaum and Jiji, at first glance, appears much more difficult to apply than the Pennes equation because $(K_{ij})_{eff}$ is a tensor and involves a description of the local microvascular geometry and flow conditions. Fortunately, it can be greatly simplified for application in many tissues because the microvascular organization can be shown to vary primarily with distance from the surface of the organ or limb. Thus this equation reduces to its one-dimensional form. In addition, there is sufficient information on the branching of the microcirculation to provide reasonable, if not accurate data on the variation of number density, size and length of the vessels with generation. From a continuity of flow equation one is then able to find the local flow velocity. This procedure is illustrated in this chapter for perhaps the most important tissue where heat transfer plays a vital role in maintaining the body's thermal balance, namely the peripheral tissue at the outer 2.5 cm of the body surface in human limbs. The purpose of this study is to show (i) how the effective conductivity of the tissue in this layer varies with depth from the skin surface due to the variation in vascular geometry and flow, (ii) to see how the temperature profile in this layer is affected by the cutaneous circulation and metabolic heat release from exercise and (iii) to examine the

range of values over which the surface heat flux can be modified due to both these physiological factors.

2.2 Three Layer Model

The vascular casts of a rabbit hind limb in [7], which are shown schematically in Figure 4, provide information on how the vascular geometry changes with tissue depth including the vessel orientation angle. A simplified but realistic three layer model for peripheral tissue has been developed. This model consists of three basic layers with distinctly different ultrastructure and thermal behavior: the deep tissue layer, the intermediate layer and the skin or cutaneous layer. Except for relative dimensions and thicknesses this basic organization is representative of surface tissue in general. Figure 5 is an idealized mathematical representation of the three layers showing the important dependent and geometric variables. The essential features of this model are summarized below.

(i) Deep tissue layer. This is a relatively thick region L_1 of thermally significant, constantly branching, counter-current arteries and veins which proceed for four or more generations as closely juxtaposed paired vessels whose dimensions diminish from 300 μm to roughly 50 μm diameter. These vessels during their final generation gradually diverge to form a periodically spaced array of transvers (terminal) vessels at the under side of the intermediate layer. In the model, the number density, size, spacing and inclination angle of the vessels vary on the average only with tissue

depth. This ultrastructure is a prescribed input in the model equations. The flow velocity along the vascular tree is determined from the prescribed vessel branching and capillary bleed-off using a continuity of flow equation. Convective and diffusive losses from the countercurrent vessels into the surrounding tissues are considered.

(ii) Transverse vessel (intermediate) layer. The intermediate layer L_2 starts when only the transverse vessels and capillaries are present in the skeletal muscle tissue and continues to the interface with the cutaneous layer. In the model the transverse vessels are assumed to be thermally insignificant and have a constant spacing which is determined by the width of the capillary beds between them. The latter are assumed to run along the length of the muscle fibers and parallel to the skin surface.

(iii) Cutaneous layer. The cutaneous layer is divided into two regions, an inner region L_3 and an outer region L_4. Warm blood at temperature θ_{bc} enters the larger thermally significant vessels of the cutaneous plexus which lie in the inner region and is perfused into the whole cutaneous layer through the vertical riser vessels connecting regions L_3 and L_4. This blood then returns to the cutaneous plexus at the local tissue temperature. Because the vertical riser vessels are thermally insignificant, the blood equilibrates with the local tissue as soon as it leaves the cutaneous plexus. This can be modeled as a distributed volumetric heat source in the inner region. The outer region contains only the vertical

riser vessels and other thermally insignificant microvessels. The arteries and veins supplying and draining the cutaneous layer are widely separated and thus experience little countercurrent heat exchange in rising through the deep tissue and intermediate layers.

2.3 Mathematical Formulation

2.3.1 Governing Equation

The new bioheat equation (5) will be applied to the idealized three layer model to find the quasi-steady temperature distribution in the peripheral tissue. Since vascular parameters such as number density, size, spacing and inclination angle of the thermally significant countercurrent vessels are assumed to vary primarily with distance from the skin surface, the blood flow velocity is also only a function of tissue depth. Subject to these simplifying assumptions, the new bioheat equation (5) reduces to an ordinary differential equation:

$$\frac{d}{dz_n}\left[K_t\left(1+\frac{\pi^2\rho_b^2 c_b^2 n a^4 u^2}{K_t^2\sigma}\ell_1^2\right)\frac{d\theta_n}{dz_n}\right]+q_n=\frac{\pi^2\rho_b^2 c_b^2 n a^4 u^2}{K_t\sigma}\ell_1\frac{d\ell_1}{dz_n}\frac{d\theta_n}{dz_n} \quad (12)$$

where z_n is measured in the direction perpendicular to the skin surface and $n = 1, 2, 3, 4$ represents the deep tissue layer, the intermediate layer and the inner and outer regions of the cutaneous layer, respectively (see Figure 5). The quantities a, n, u, ℓ_1 and σ are functions of z_n. The term on the right hand side is due only to the change of the inclination of the vessels. In regions where the blood vessels are primarily perpendicular to the skin surface, such

as the transverse vessels of the intermediate layer and the vertical riser vessels of the cutaneous layer, this term vanishes.

Equation (12) may be put in a more convenient form by defining an inflow Peclet number P_{e0} in the deep tissue based on the inflow velocity u_0 and radius a_0

$$P_{e0} = \frac{2\rho_b c_b a_0 u_0}{K_b} \tag{13}$$

Then equation (12) can be written in a non-dimensional form in which the coefficient of the derivative terms can be separated into dimensionless products of known functions which prescribe the variation of vascular geometry with depth from the skin surface and the inflow parameter P_{e0} describing the inflow conditions in the deep tissue layer. This separation permits us to substitute different input flow conditions into the governing equation and study the heat transfer of a specific surface tissue under a wide range of physiological conditions.

The three layer model will now be converted into a coupled dimensionless boundary value problem for each layer with appropriate boundary and matching conditions. The following dimensionless quantities are defined:

coordinate, $\tilde{z}_n = z_n/L_n$

temperature, $\tilde{\theta}_n = (\theta_n - T_s)/(T_0 - T_s)$

distributed heat source, $\lambda_n = q_n L_n^2/K_t (T_0 - T_s)$

Equation (12) becomes:

$$\frac{d}{d\tilde{z}_n}\left[(1 + A(\tilde{z}_n)P_{e0}^2)\frac{d\tilde{\theta}_n}{d\tilde{z}_n}\right] + \lambda_n = B(\tilde{z}_n)P_{e0}^2 \frac{d\tilde{\theta}_n}{d\tilde{z}_n} \tag{14}$$

where

$$A(\tilde{z}_n) = \frac{\pi^2}{4}\left(\frac{K_b}{K_t}\right)^2 \frac{n a^4 \ell_i^2}{\sigma a_o^2}\left(\frac{u}{u_o}\right)^2 \tag{15}$$

$$B(\tilde{z}_n) = \frac{\pi^2}{8}\left(\frac{K_b}{K_t}\right)^2 \frac{n a^4}{\sigma a_o^2}\left(\frac{u}{u_o}\right)^2 \frac{d\ell_i^2}{d\tilde{z}_n} \tag{16}$$

Note that the functions $A(\tilde{z}_n)$ and $B(\tilde{z}_n)$ involve products of either properties of tissue and blood, functions of geometry varying with depth or the dimensionless velocity ratio u/u_o.

The continuity of flow relation in a branching countercurrent artery can either be described by discrete branchings or alternatively by a continuous variation of the form

$$\frac{d}{ds}(n a^2 u) = -2 n a g \tag{17}$$

where s measures distance along the vessel axes, and g is a bleed-off rate per unit vessel surface area from the countercurrent artery or to the countercurrent vein. This same equation applies to the countercurrent vein if the small flow losses to the lymphatic circulation are ignored. When the bleed-off per unit distance from the branching countercurrent network is constant, the blood supply to the capillaries in the deep tissue and intermediate layers will be uniform. This is a reasonable approximation because vascular casts have shown that the number density of capillary beds is nearly uniform throughout the skeletal muscle tissue [7]. Furthermore this bleed-off plays only a secondary role compared to the primary mechanism of incomplete countercurrent heat exchange in determining the effective conductivity. Under these conditions the right hand side of equation (17) is constant. Since all the blood entering at

$\tilde{z}_1 = 0$ must eventually leave the arterial side at the terminus of the transverse vessels at the top of the intermediate layer, this constant has the value

$$2\pi a g = \frac{\pi_0 a_0^2 u_0}{S_{DI}} \tag{18}$$

where S_{DI} is the total length of the countercurrent arterial network from its entrance at the base of the deep tissue layer. The dimensionless velocity ratio at any distance s along the branching network is then from (17) given by

$$\frac{u}{u_0} = \left(\frac{\pi_0 a_0^2}{\pi a^2}\right)\left(1 - \frac{s}{S_{DI}}\right) \tag{19}$$

For conditions of uniform capillary perfusion u/u_0 is thus seen to be only a function of vascular geometry and the functions $A(\tilde{z}_n)$ and $B(\tilde{z}_n)$ are independent of the inflow velocity u_0 or Peclet number P_{e0}.

For conditions stated above, equation (14) can now be written in a final compact form where the effect of vascular geometry and blood supply to the deep tissue and intermediate layers have been separated

$$(1 + P_{e0}^2 A)\frac{d^2\tilde{\theta}_n}{d\tilde{z}_n^2} + P_{e0}^2\left(\frac{dA}{d\tilde{z}_n} - B\right)\frac{d\tilde{\theta}_n}{d\tilde{z}_n} + \lambda_n = 0 \tag{20}$$

The functions A and B can be constructed separately for a given tissue, and the behavior of equation (20) examined for this tissue by simply varying P_{e0} and λ_n. The coefficient of the first term in equation (20)

$$\frac{K_{eff}}{K_t} = 1 + P_{e0}^2 A(\tilde{z}_n) \tag{21}$$

is the enhancement in conductivity due to the blood flow and bleed-off in the thermally significant countercurrent

vessels, and is equivalent to those given in equations (6) and (11) for the one-dimensional case.

2.3.2 Vascular Input Parameters and Variation in Effective Thermal Conductivity

The next task is to determine the variables A and B as functions of tissue depth and examine the variation of the effective tissue conductivity in each layer. Simple functional forms have been proposed in references [8] and [9] for the spatial variation of n, a, σ and ℓ_1 in the deep tissue layer. These functional forms, which permit a smooth prescription of input data, are given by

$$n(\tilde{z}_1) = n_0 (1 - c_1 \tilde{z}_1)^{-c_2} \tag{22}$$

$$a(\tilde{z}_1) = a_0 (1 - c_3 \tilde{z}_1)^{c_4} \tag{23}$$

$$\sigma(\tilde{z}_1) = \frac{\pi}{\cosh^{-1}(c_5 + c_6 \tilde{z}_1^{c_7})} \tag{24}$$

$$\ell_1(\tilde{z}_1) = \cos[c_8 (1 - \tilde{z}_1)] \tag{25}$$

From (19) the blood velocity in the countercurrent artery or vein is

$$U(\tilde{z}_1) = U_0 \frac{(1 - c_1 \tilde{z}_1)^{c_2} (1 - \frac{S}{S_{DI}})}{(1 - c_3 \tilde{z}_1)^{2c_4}} \tag{26}$$

The quantities c_1, c_2, c_3, c_4, c_5, c_6, c_7, c_8 and n_0, a_0, S_{DI} describing the vascular anatomy of peripheral tissue shown in Table 1 are based on approximate measurements taken from the rabbit hind limb in [7]. The sensitivity of the temperature profiles to the variation in these coefficients

was explored in detail in the parametric studies performed in Dagan et al. [9] which showed that their most important influence is in the lower part of the deep tissue layer. These results can be made representative of peripheral tissue in other limbs and species by adjusting the thicknesses of the tissue layers L_n and only the initial dimensions of the countercurrent vessels at the entry to the deep tissue layer. The functional form of the branching and diminution in vessel size with generation should not vary significantly from one peripheral tissue to another. Also shown in Table 1 are the values of the various blood-tissue properties and the different layer thicknesses.

The variation of the vascular parameters with depth in the deep tissue is summarized in Table 2. Also shown is the variation of the functions A and B for the prescribed vascular geometry. The number density n varies slowly at first since the vessel length diminishes with each generation, and the longest vessels are in the first two generations. Similarly, vessel radius a changes slowly at first and then rapidly decreases as n grows. The shape factor σ which describes the thermal equilibration of the vessels depends on the local ratio e/a and varies little until the final two generations where the countercurrent vessels start to diverge before leading to the roughly periodically spaced transverse vessels.

On the right hand side of Table 2 is shown the variation in the effective conductivity for three different inflow

Peclet numbers characterizing the basal state $P_{e_0} = 60$ and two levels of increasing exercise. There are several crucial observations. First, K_{eff} rapidly decreases toward its conduction value as vessel size decreases and most of the enhancement in heat transfer due to blood flow occurs in vessels between 100 μm and 300 μm diameter. Second, in the basal state flow rates are too small to produce large increases in conductivity. This would suggest that in a supine state in a hot environment the body must develop other mechanisms such as increasing cutaneous blood flow rate and sweating to reject heat. Third, large enhancements in effective conductivity are possible during exercise to promote the removal of heat from deep tissue.

The results of the new bioheat equation are just the reverse of what one would predict on the basis of Pennes bioheat equation. There is virtually no enhancement in conductivity in tissue regions where the largest vessels are under 100 μm, such as the intermediate layer. Capillary perfusion affects tissue heat transfer only in so much as it increases the blood supply to the larger countercurrent vessels in the peripheral microcirculation. There is no blood-tissue heat transfer in the smallest microvessels per se.

Tables similar to Table 2 could be constructed for both the transverse vessels of the intermediate layer and the vertical riser vessels in the cutaneous layer. The calculated values of A in these regions (B is identically zero since

these vessels are perpendicular to the skin surface) are small and there is less than a one percent change in conductivity in these regions for all flow conditions. The variation in A and B throughout the peripheral tissue is shown in Figure 6.

2.3.3 Model Simplification and Solution Procedure

It is evident from the above discussion that a much simpler form of model equation can be used in both the intermediate and cutaneous layers. In the intermediate layer, equation (20) reduces to

$$\frac{d^2\tilde{\theta}_2}{d\tilde{z}_2^2} + \lambda_2 = 0 \qquad (27)$$

Similarly, in the upper portion of the cutaneous layer L_4 one can use an ordinary heat conduction equation since there is little metabolically generated heat because of the relatively little muscle activity

$$\frac{d^2\tilde{\theta}_4}{d\tilde{z}_4^2} = 0 \qquad (28)$$

The treatment of the lower portion of the cutaneous layer is more subtle. Provided that the warm blood entering the cutaneous plexus rises through the muscle tissue via the widely separated large vessels that supply this layer from the central artery of the limb, it experiences little counter-current heat exchange. This blood enters the cutaneous plexus at temperature θ_{bc} and undergoes an instantaneous equilibration to the local tissue temperature θ_3 upon entering the small vertical riser vessels that supply the upper portion of the cutaneous layer. For the same reason the blood reentering

the veins of the cutaneous plexus must also be at the local tissue temperature. The strength of this heat source per unit volume in the inner region is

$$q_c = W_{bc} \rho_b c_b (\theta_{bc} - \theta_3) \tag{29}$$

where W_{bc} is the volumetric bleed-off rate to the thermally insignificant vertical riser vessels emanating from this region. If one neglects metabolic heat production for the same reason as stated previously, the dimensionless governing equation for this inner cutaneous layer is

$$\frac{d^2\tilde{\theta}_3}{d\tilde{z}_3^2} + F R P_{e0} (\tilde{\theta}_{bc} - \tilde{\theta}_3) = 0 \tag{30}$$

where

$$F = \frac{\pi n_0 a_0 L_3 K_b}{2 K_t} \tag{31}$$

and R is defined as the ratio of blood supplied to the cutaneous layer to the blood supplied to the combined deep tissue and intermediate layers

$$R = \frac{Q_c}{Q_{DI}} \tag{32}$$

R is an important physiological parameter describing the distribution of blood supplied to different tissue layers according to the combined effect of environmental temperature and levels of muscle activity of the body. The distribution of blood flow between the cutaneous and subcutaneous layers must be treated as a prescribed input in the present model since the flow to the cutaneous layer is largely controlled by the blood temperature from all parts of the body as integrated by the hypothalamus [13], and to a much lesser degree

the local effect of the skin temperature [14], while the blood supply to the muscle tissue beneath this layer depends on the oxygen consumption of this tissue. Thermoregulatory models for the blood temperature integrated by the hypothalamus must be based on a model for whole body heat transfer. Models of this type have been developed by Hammel [15], Huckaba et al. [16] and most recently Arkin and Shitzer [17].

The dimensionless temperature $\tilde{\theta}_{bc}$ of the blood from the central artery when it arrives at the cutaneous plexus depends on the blood flow rate into the cutaneous layer Q_c. In the supine resting state in a cool environment, when this flow is very slow, blood entering this layer will have equilibrated to the local tissue temperature. In this limit, $\tilde{\theta}_{bc} = \tilde{\theta}_3(0)$ where $\tilde{\theta}_3(0)$ is the dimensionless local tissue temperature that would be obtained at the base of the cutaneous layer if there were no blood perfusion in this layer. In the other limit, maximum vasodilation, the flow rate to the cutaneous layer is so large that there is little thermal equilibration of the blood before it enters the cutaneous layer. In this limit the dimensionless blood temperature $\tilde{\theta}_{bc} = 1$, which implies that the blood temperature θ_{bc} is equal to the local arterial supply temperature in the deep tissue. The increase of Q_c, which is the product of R and Q_{D1}, is equivalent to an increase in R P_{e0}. It is well known that a constant area tube flow, which loses heat to a roughly uniform temperature environment, has an axial temperature which decays exponentially as an inverse function of the

Peclet number and thus the corresponding integrated heat loss along the tube is linearly proportional to the Peclet number. Therefore it is reasonable to assume as a first approximation a simple linear relationship between $\tilde{\theta}_{bc}$ and R P_{e0} ,

$$\tilde{\theta}_{bc} = c_9 + c_{10} R P_{e0} \tag{33}$$

The constants c_9 and c_{10} can be determined from the two limiting cases just described. The values of c_9 and c_{10} found in this manner are 0.093, 0.001, respectively and the maximum value of R P_{e0} is 720.

The dimensionless distributed heat source in the deep tissue and intermediate layers, λ_1 and λ_2, originate from the metabolic heat production in these regions. Factors such as activity level, diet, age, sex and tissue type influence metabolic heat production. In addition, it can be a function of environmental factors because of the temperature homeostasis of the body [18]. For a specific surface tissue organization under fixed steady state environmental conditions, the metabolic heat production is mainly controlled by the activity level of voluntary or involuntary muscle contraction. Shivering is an asynchronous involuntary muscle activity that can be used as a thermoregulatory response to raise body core temperature in a cold environment. Because metabolic heat production is directly proportional to the oxygen consumption, and the oxygen uptake is related to the blood flow rate in the region [14], the dimensionless metabolic heat production and the inflow Peclet number are coupled and a linear relationship between them can be assumed.

Since the metabolic heat release is nearly uniform throughout the deep tissue and the intermadiate layers, $q_1 = q_2$. Thus,

$$\lambda_1 = c_{11} + c_{12} P_{e0} \tag{34}$$

and $\lambda_2 = \lambda_1 (L_2^2 / L_1^2)$. If one uses as the two limiting cases of the value $\lambda_1 = 0.02$ for the supine resting state and 1 for moderate exercise, c_{11} and c_{12} are found to be -0.307 and 0.005, respectively. This corresponds to $P_{e0} = 60$ in the resting state and $P_{e0} = 240$ during moderate exercise.

The boundary value problem just described can be solved by first analytically solving equations (27), (28) and (30) for the intermediate and cutaneous layers and satisfying matching boundary conditions for the temperature and heat flux at the interfaces between them. This solution leads to a compatability equation:

$$\frac{d\tilde{\theta}_1(1)}{d\tilde{r}_1} = \frac{L_1}{L_2}\left\{\left[\left(\frac{1}{2} + \frac{L_3}{L_2\sqrt{FRP_{e0}}}\right)\lambda_2 - \tilde{\theta}_1(1) + \tilde{\theta}_{sk}\right]\cdot\left(1 + \frac{L_3\sqrt{FRP_{e0}}}{L_3}\right)e^{\sqrt{FRP_{e0}}} + \right.$$
$$+\left[\left(\frac{1}{2} - \frac{L_3}{L_2\sqrt{FRP_{e0}}}\right)\lambda_2 - \tilde{\theta}_1(1) + \tilde{\theta}_{sk}\right]\cdot\left(1 - \frac{L_3\sqrt{FRP_{e0}}}{L_3}\right)e^{-\sqrt{FRP_{e0}}} - 2\tilde{\theta}_{sk}\Big\}\Big/ \tag{35}$$
$$\left\{\left(1 + \frac{L_3}{L_2\sqrt{FRP_{e0}}}\right)\left(1 + \frac{L_3\sqrt{FRP_{e0}}}{L_3}\right)e^{\sqrt{FRP_{e0}}} + \left(1 - \frac{L_3}{L_2\sqrt{FRP_{e0}}}\right)\left(1 - \frac{L_3\sqrt{FRP_{e0}}}{L_3}\right)e^{-\sqrt{FRP_{e0}}}\right\}$$

relating the temperature and temperature gradient at the interface between the deep tissue and intermediate layers. The curves for A and B in Figure 6 are then approximated by simple polynomials and the governing equation for the deep tissue layer, equation (20) with $n = 1$, is integrated numerically by satisfying the known initial

temperature but a guessed initial temperature gradient at $\tilde{z}_1 = 0$. Condition (35) is then used as an end point constraint to determine the correct value of the guessed initial temperature gradient.

2.4 Results and Discussion

Since both $\tilde{\theta}_{bc}$ and $\lambda_{1,2}$ can be related to P_{e0} and R, only two key dimensionless parameters enter in the governing equations for the three layer model, the inflow Peclet number P_{e0} at the base of the deep tissue layer and the ratio R that describes the relative magnitudes of the blood supply to the cutaneous and combined deep tissue and intermediate layers respectively.

The inflow Peclet number is mostly affected by the level of exercise. This blood flow is largely controlled by the oxygen demand of the skeletal muscle tissue. For the supine resting state a typical inflow velocity is about 2.5 cm/sec [19], which corresponds for the vascular parameters chosen to a P_{e0} of 60. For moderate exercise this can increase by a factor of four to an inflow Peclet number of 240 [20].

It is generally accepted that the control of the cutaneous blood flow is a major thermoregulatory effector process. In the supine resting state and neutral environment the cutaneous layer is vasoconstricted and the value of R is approximately 0.01. For exercise in a neutral environment Q_c will increase in response to the "integrated blood temperature" in the hyperthalamus and Q_{DI} will increase in response to the increased oxygen demand. R = 1.0 is a reasonable

estimate for the blood flow distribution under these conditions of moderate exercise. During conditions of maximum vasodilation the cutaneous circulation can be increased by a factor of 20 and the blood supply to the skeletal muscle tissue somewhat reduced if the cardiac output is insufficient to meet the demands of heat stress and exercise. A reasonable maximum value of R for the peripheral layer chosen is about 3.0.

In Figures 7 and 8 the representative solutions for the peripheral tissue temperature profiles are plotted. The location of the interface between layers is indicated by a vertical dashed line. Figure 7 shows the effect of increasing the blood flow supply or the inflow Peclet number P_{eo} to the deep tissue. In the supine resting state (P_{eo} = 60) the profile is linear since there is both little enhancement in conductivity in the deep tissue and insufficient blood flow to the cutaneous plexus for the blood entering this layer to depart significantly from the local tissue temperature. Thus there is relatively little heat release by the cutaneous circulation. At the higher values of P_{eo} there is a significant rise in temperature in the deep tissue primarily due to the enhanced conductivity arising from the larger countercurrent vessels in the deeper portion of the peripheral tissue as already noted in the discussion of Table 2 and Figure 6. At the smaller value of R = 0.01 the temperature in the outermost 10 mm of tissue is nearly linear indicating that this entire region behaves as a conduction

layer when the cutaneous circulation is vasoconstricted. At a intermediate value of R = 1.0 there is sufficient blood flow to the cutaneous plexus when the inflow Peclet number is large for the blood entering this layer to have only undergone partial precooling in the deep tissue and thus provide a moderate heat source in the lower portion of the cutaneous layer.

Figure 8 provides a more detailed examination of the role of the cutaneous circulation in promoting surface heat transfer. As is evident from equation (33) the blood supply to the cutaneous plexus is proportional to the product R P_{eo} and not just R itself. Thus both R and P_{eo} have to be large before the blood supply to the cutaneous layer is sufficiently high for its temperature to depart significantly from the local tissue temperature. When this occurs there is both substantial heat deposited in the cutaneous tissue and a large increase in the surface temperature gradient produced to reject this heat. The skin at this time has a hot flushed appearance arising from the large amount of warm blood that is delivered to the surface without significant precooling.

Another important effect which is not readily evident in Figures 7 and 8 is the role of metabolic heat production. In the present model it is assumed that this heat release is uniformly distributed in the deep tissue and intermadiate layers and proportional to the muscle tissue blood supply P_{eo}. Because the enhanced conductivity due to the countercurrent blood flow produces a similar change in the temperature

profiles in the deep tissue as metabolic heat release, it is difficult to distinguish these two mechanisms. Both lead to an increase in deep tissue temperature. However, the substantial elevation in temperature in the region surrounding the interface between the deep tissue and intermediate layers is primarily due to metabolic heat release, since as previously noted there is little increase in the effective conductivity due to blood flow in this region. For higher values of P_{eo} not shown it is possible to have a temperature maximum in the deep tissue layer, a result noted previously by several authors (17, 21).

Figure 9 shows how the heat flux or surface temperature gradient varies as a function of the distribution of the blood supply to the cutaneous and subcutaneous tissue and the deep tissue blood supply. The importance of having both P_{eo} and R increase during moderate exercise is clearly seen in Figure 9. As stated earlier very high flow rates to the cutaneous layer are required to minimize the precooling of the cutaneous blood flow in crossing the deep tissue layer. The ability of the body to reject metabolic heat is primarily a function of the cutaneous circulation, but significant increases can result due to the profile changes caused by the heat production itself when the cutaneous circulation is vasoconstricted but the temperature is elevated in the intermediate layer due to metabolic heat generation in the skeletal muscle tissue as discussed at the end of the last paragraph. This behavior is clearly evident in Figure 9 where

it is observed that there is a near doubling of the surface heat flux at small values of R. This mechanism provides for a substantial increase in the rejection of heat during exercise in a cold environment where one would expect the cutaneous blood flow to be very low. When one examines the entire range of thermoregulatory control due to blood flow in Figur 9, it is evident that the naked body in a well ventilated environment where there is little thermal resistance at the skin surface should be capable of increasing its surface heat transfer by roughly a factor of ten without having to resort to sudomoter control or sweating.

2.5 Concluding Remarks

This study and the study of the detailed arterio-venous temperature differences in the countercurrent vessels of the peripheral tissue by Dagan et al. [9] provide some fundamental new insights into the physiological function and organization of surface tissue. Although the small local arterio-venous temperature difference does not decrease significantly throughout the deep tissue layer, this study shows that the blood flow in both the intermediate layer and the outer portion of the deep tissue layer provides very little enhancement in conductivity although the magnitude of the blood perfusion is roughly the same as in the deeper tissue. The body is thus able to conserve heat in a cold environment by providing a much thicker outer conduction layer than had been previously realized. If it were not for the countercurrent organization of the microvasculature in

the deep tissue warm blood from the central arterial supply vessels would be delivered to the tissue just beneath the cutaneous plexus and a large surface heat loss would occur under resting conditions. Furthermore, it now seems clear why the countercurrent microvessels first diverge when their dimensions are approximately 50 μm. It is at this size that these vessels first become thermally insignificant and no longer function as a countercurrent heat exchanger.

The large proliferation of thermally insignificant vessels in the intermadiate layer would also appear to serve an important physiological function. These vessels, which one would not want to conduct heat in the resting state for the reasons just given, most likely provide for a large generation of heat in the skeletal muscle during exercise. Their close proximity to the surface thus provides for a significant augmentation of the heat loss through the skin which is primarily controlled by the cutaneous circulation. Finally, rather large flow rates to the cutaneous circulation are required if the blood entering the cutaneous layer is to not undergo substantial precooling in the underlying tissue. The cutaneous circulation serves two vital physiological functions. It not only cools blood from the core of the body but also is able to significantly elevate the skin surface temperature and thereby greatly enhance the removal of metabolically generated heat in the muscle tissue beneath it. The mathematical model developed herein, is the first to my knowledge which attempts to relate the temperature of the

blood entering the cutaneous layer to the blood flow rate in this layer.

The peripheral tissue heat transfer model just described will be utilized in the next chapter to develop a model for whole limb heat transfer. The one-dimensional form of equation (20) can be easily modified to take account of the curvature in a radial coordinate system and then be applied to determine the radial temperature profile in the muscle tissue of the limb. The basic problem is to show how the heat exchange from the large countercurrent central vessels, which run the length of the limb and which are far from thermal equilibrium with the local tissue, can be coupled with microvascular heat exchange in the muscle tissue where the arterial and venous blood in the thermally significant microvessels depart only slightly from the local tissue temperature. When the governing equation for the axial temperature variation of the central artery and vein is combined with the local conduction solution for the temperature field in the vicinity of these vessels, one obtains a matching condition which relates the average core temperature for the central vessels to local average tissue temperature of the surrounding muscle tissue. A new prototype model for whole limb heat transfer based on these ideas will be presented in the next chapter.

3. New Model for an Entire Limb Heat Transfer

3.1 Background

Existing models of limb heat transfer fall into three broad categories (a) those that attempt to model the radial temperature distribution, (b) those that attempt to model the axial temperature distribution in the central artery and vein and (c) multi-compartment models. Both models (a) and (c) have been based on the Pennes bioheat equation (1). The prototype for the model in (a) is Pennes's classic paper [1] for determining the radial temperature profile in the human forearm. Axial conduction is neglected in [1] and various steady state solution profiles are obtained by solving equation (1) for different values of the blood perfusion parameter subject to a radiation boundary condition at the surface. Aside from the axial asymmetry, the theory and experiments provided reasonable agreement except that the theoretically predicted profiles had the wrong curvature. According to the analysis in Chapter 2, it is believed that this is due to the radial variation in the effective thermal conductivity due to the microvascular geometry and blood flow. This variation is an intrinsic part of the bioheat equation of Weinbaum and Jiji.

The prototype of models of type (b) is the well known paper of Mitchell and Myers [22]. This model treats the central artery and vein as a one-dimensional countercurrent heat exchanger which experiences heat losses to a uniform temperature external environment along its length. There is

no extremity and the arterial and venous temperatures are set equal at the end of the limb. No model has attempted to combine the axial and radial temperature distributions in a continuous manner or treat the skin surface temperature as a continuously varying unknown. A step in this direction are the multi-compartment models proposed for whole body heat transfer by Wissler [23] and the more recent related work of Arkin and Shitzer [17]. In these models of type (c) the upper and lower arms and legs and their extremities are treated as different radii cylinders. Each cylinder is composed of concentric layers of tissue with different capillary perfusion rates and the radial profile is determined from the Pennes equation. There is no axial variation of temperature except at the junction between cylinders where the overall energy balance on the blood entering and leaving the cylinder must be satisfied.

3.2 New Model Description

3.2.1 Novel Features of the New Model

A new generation of model for whole limb heat transfer including the extremity will be proposed herein. This model is a radical departure from the macroscopic models described above in that it will be based on an approximate model representing the actual microvascular and macrovascular organization of the limb in which the spatial organization of the vascular geometry is prescribed. The model should permit (i) a greatly improved quantitative interpretation of physiological

measurements of the steady state thermal behavior of the limb and (ii) a more accurate prediction of whole limb heat transfer under thermoneutral conditions and conditions of thermal stress and exercise. This model will include a number of fundamental novel features which have not appeared heretofore in theoretical studies of whole limb heat transfer. These include:

(a) an arbitrary variation in cross-sectional area with axial distance of the limb;

(b) an unknown axial distribution of surface temperature as well as central artery and vein temperatures, which will be determined as part of the solution procedure;

(c) a continuity of flow relationship which allows for a continuous bleed-off from the central artery and vein and distribution to the muscle and cutaneous circulations and the extremity;

(d) a microvascular model for radial temperature distribution based on the bioheat equation of Weinbaum and Jiji;

(e) a model for relating the temperature of arterial blood entering the cutaneous plexus and metabolic heat generation in the muscle tissue to microvascular blood flow;

(f) a model for determining the heat loss from the extremity.

3.2.2 Model Geometry

Figure 10 is a simplified diagram showing the essential elements, symbols and coordinates of a length segment of the

arm and the extremity in the mathematical model. Three basic regions of the arm are identified, a central region or core of radius r_c containing the major artery and vein that run the length of the limb, a surrounding layer of muscle and fat tissue which extends to within roughly 2 mm of the skin surface, and a cutaneous layer with both its inner and outer regions as described previously in Chapter 2. Heat transfer at the skin surface is characterized by convection and radiation coefficients h_c and h_r and there is also heat loss through evaporation q_{ev}. The limb with its central countercurrent axial vessels is assumed to be axisymmetric and the cross-sectional area can be varied arbitrarily by introducing a shape factor $G(x)$ which scales the initial radius of the arm r_{si} so that the local radius is given by $G\, r_{si}$. It is also assumed that the radii of the central countercurrent axial vessels a_a and a_v and the radius of the core r_c scale by the same factor $G(x)$ as one proceeds along the axis of the arm. The central artery and vein temperatures at the entrance to the extremity, $T_a(L)$ and $T_v(L)$, are unknown and are to be determined from the solution of the model. In contrast, the difference in these two temperatures can be found directly from a model for the heat loss from the extremity provided the blood flow to the extremity is prescribed. The essential features for each region of the arm are summarized below:

(i) The core. The central region or core contains the countercurrent central artery and vein and the immediate surrounding tissue. Two important features of the central

artery and vein are that their temperatures T_a and T_v depart significantly from the local average tissue temperature θ and that this average temperature is not a simple average of T_a and T_v because the vein is in general two to three times as large as the artery. The average temperature at the edge of the core will be determined by the local conduction field about these vessels and can be shown to be equal to the far field temperature in the local cross-sectional plane. This far field temperature will also be shown to be equal to the average tissue temperature that is obtained by integrating the local tissue temperature over the cross-sectional plane. The radial blood flow leaving the central artery and returning to the central vein will be assumed to be proportional to (i) the local cross-sectional area of the muscle tissue and to (ii) the local perimeter of the skin surface. In the latter the blood is supplied by isolated large riser vessels that supply and drain the cutaneous plexus. The fraction of the total blood flow to the limb that enters the arm as opposed to the extremity ψ, is further divided between the muscle and cutaneous circulations by introducing a second parameter ω which describes the fraction of the radial blood flow from the central artery that enters the muscle tissue. Thus, if $\pi u_{ai} a_{ai}^2$ is the total blood supply to the arm and extremity, $\pi u_{ai} a_{ai}^2 \omega\psi$, $\pi u_{ai} a_{ai}^2 (1-\omega)\psi$ and $\pi u_{ai} a_{ai}^2 (1-\psi)$ represent the total blood supply to the muscle tissue of the arm, the cutaneous tissue of the arm and the total blood flow to the extremity respectively. The parameters ω and ψ are prescribed and depend on the level of

exercise, the temperature of the skin and the central regulation of the hypothalamus and spinal core.

(ii) The muscle tissue. The muscle tissue, which comprises the major volume fraction of the arm, will be described by the bioheat equation of Weinbaum and Jiji and a microvascular model whose geometry and flow vary with distance from the skin surface. One of the important results derived in the new model for peripheral tissue heat transfer in Chapter 2 is that the effective conductivity of the tissue varies substantially in the radial direction due to the branching and diminution in size of the countercurrent vessels of the microvasculature as one proceeds from the larger vessels in the deep tissue towards the surface. The metabolic heat generation of the muscle tissue will be assumed to be proportional to the oxygen consumption and the latter assumed proportional to the blood supply to the muscle. The intermediate layer introduced in Chapter 2, which is comprised largely of thermally insignificant microvessels, can be treated as part of the muscle tissue. A subcutaneous fat layer could also be introduced, but this is an unnecessary complication since its effective conductivity would not differ significantly from non-vascularized tissue so it only acts as a conduction layer for the heat transfere.

(iii) The cutaneous layer. The cutaneous layer is divided into two thin regions: the inner region with the larger thermally significant vessels of the cutaneous plexus and an outer region with small riser vessels and vertical anastomoses. Warm blood at temperature θ_{bc} enters the

cutaneous plexus and is then perfused into the upper portion of the cutaneous layer through vertical riser vessels and returns to the cutaneous plexus at the local tissue temperature. This warm blood perfusion can be modeled as a distributed volumetric heat source in the inner region as described in detail in Chapter 2. The outer region, in the absence of thermally significant vessels, behaves as a pure conduction layer and exchanges heat at its surface with the surroundings by convection, radiation and evaporation. Evaporation heat removal includes two mechanisms: the heat loss by diffusion of water through the skin, and the heat loss by sweating secretion which is controlled by the sudomoter regulatory system.

3.3 Mathematical Formulation

3.3.1 Core Flow and Energy Balance

(i) Continuity equation. Blood is supplied radially from the central artery to the muscle and cutaneous layers through two separate systems of vessels. Experimental measurements indicate that the cutaneous layer and the muscle tissue have vastly different volumetric blood perfusion rates that are, however, nearly uniform throughout the arm in each tissue region. Thus, the local blood bleed-off rates to muscle and to the cutaneous layer per unit length of the central artery, $P_m(x)$ and $P_s(x)$, can be related to the variation in local cross-sectional area $\pi G^2 r_{si}^2$ for the muscle tissue and the local perimeter $2\pi G r_{si}$ for the cutaneous layer

$$P_m(x) = \pi \psi \omega a_{ai}^2 u_{ai} \frac{G^2(x)}{\int_0^L G^2(z)\,dz} \tag{36}$$

and

$$P_s(x) = \pi \psi (1-\omega) a_{ai}^2 u_{ai} \frac{G(x)}{\int_0^L G(z)\,dz} \tag{37}$$

where z serves as a dummy axial integration variable. Consider a differential length element dx of the central artery. The conservation of fluid mass gives the change of volumetric blood flow rate in the axial direction

$$\pi \frac{d}{dx}(a_a^2 u_a) = -(P_m + P_s) \tag{38}$$

or

$$\frac{d}{dx}(a_a^2 u_a) = -\psi a_{ai}^2 u_{ai}\left[\frac{\omega G^2}{\int_0^L G^2 dz} + \frac{(1-\omega) G}{\int_0^L G\,dz}\right] \tag{39}$$

Knowing the volumetric flow rate at the entrance of the arm, and the fraction of this total blood supply that enters the extremity, one can show by integrating equation (39) to its far end that the local flow rate of the central artery is given by

$$a_a^2 u_a = a_{ai}^2 u_{ai}\left\{\psi\left[\frac{\omega \int_0^L G^2 dz}{\int_0^L G^2 dz} + \frac{(1-\omega)\int_0^L G\,dz}{\int_0^L G\,dz}\right] + (1-\psi)\right\} \tag{40}$$

(ii) Energy equation. Consider now the energy balance on the differential length element dx of the central artery. Energy leaves the central artery both through a radial bleed-off into the terminal arteries that supply the muscle and cutaneous circulations and conductive heat transfer through the vessel wall. This combined heat loss is then equated to the change in energy convected by the blood in the central artery over the length element dx. When the

continuity equation (38) is taken into account, the energy equation for the central artery can be simplified to

$$\pi \rho_b c_b a_a^2 u_a \frac{dT_a}{dx} = -q_a \tag{41}$$

where q_a is the conductive loss per unit length of the artery.

A similar equation can be obtained for central vein where the local convective energy flux is $\pi \rho_b c_b a_v^2 u_v T_v$. However, since the lymphatic circulation involves at most a few percent of the capillary bleed-off from the countercurrent arteries and veins in the microcirculation, the volumetric flow rate of the paired central artery and vein at a given axial location is almost the same, i.e., $\pi a_a^2 u_a = \pi a_v^2 u_v$. Thus, the axial variation of blood temperature in the central vein is

$$\pi \rho_b c_b a_a^2 u_a \frac{dT_v}{dx} = -q_v \tag{42}$$

where q_v is the conductive loss per unit length of vein.

(iii) Derivation of mean tissue temperature for core. Consider the local temperature field in the cross-sectional plane perpendicular to the countercurrent pair of vessels of different radii as shown in Figure 11. The origin of coordinates is located such that

$$\sqrt{e_a^2 - a_a^2} = \sqrt{e_v^2 - a_v^2} = \alpha \tag{43}$$

where

$$e_a + e_v = e \tag{44}$$

is the vessel spacing and T_{oo} is the temperature at this

origin. The local temperature field in the vicinity of the central artery and vein is determined by the conduction field in the local cross-sectional plane. This classic solution in bicircular coordinates gives the temperature difference between the surrounding tissue T and T_{∞} and assumes that the heat conducted through the vessel walls is almost equal for each vessel in the vessel pair ($q_a \simeq q_v = q$)

$$T - T_{\infty} = \frac{q}{4\pi K_t} \ln\left[\frac{y^2 + (z-a)^2}{y^2 + (z+a)^2}\right] \tag{45}$$

Applying equation (45) at $y = 0$ at the innermost point of each vessel, one obtains

$$T_a - T_{\infty} = \frac{+q}{2\pi K_t} \cosh^{-1} M_a \tag{46}$$

and

$$T_v - T_{\infty} = \frac{-q}{2\pi K_t} \cosh^{-1} M_v \tag{47}$$

where

$$M_a = \frac{e_a}{a_a} = \frac{(e/a_a)^2 - (a_v/a_a)^2 + 1}{2(e/a_a)} \tag{48}$$

and

$$M_v = \frac{e_v}{a_v} = \frac{(e/a_v)^2 - (a_a/a_v)^2 + 1}{2(e/a_v)} \tag{49}$$

The sum and difference of the above equations give

$$T_a - T_v = \frac{q}{2\pi K_t}(\cosh^{-1} M_a + \cosh^{-1} M_v) \tag{50}$$

and

$$T_a + T_v - 2T_{\infty} = \frac{q}{2\pi K_t}(\cosh^{-1} M_a - \cosh^{-1} M_v) \tag{51}$$

The conductive heat transfer between the central artery and vein can be found to a first approximation from equation (50)

$$q = \sigma_c K_t (T_a - T_v) \tag{52}$$

where σ_c is a shape factor defined by

$$\sigma_c = \frac{2\pi}{\cosh^{-1} M_a + \cosh^{-1} M_v} \tag{53}$$

Since $(T-T_{oo})$ is an anti-symmetric function of z,

$$P.V. \int_{-\infty}^{\infty}\int_{-\infty}^{\infty} (T - T_{oo})\, dz\, dy = 0 \tag{54}$$

it follows that if one defines a tissue mean temperature θ, then $\theta = T_{oo}$. Therefore, T_{oo} or θ can be calculated from equations (51), (52) and (53)

$$\begin{aligned} \theta &= \frac{1}{2}\left[(1-\beta) T_a + (1+\beta) T_v\right] \\ &= \frac{1}{2}(T_a + T_v) - \frac{\beta}{2}(T_a - T_v) \end{aligned} \tag{55}$$

where

$$\beta = \frac{\cosh^{-1} M_a - \cosh^{-1} M_v}{\cosh^{-1} M_a + \cosh^{-1} M_v} \tag{56}$$

It is recorgnized from (55) and (56) that when the vessel radii are different $\beta \neq 0$ and the tissue mean temperature is not the arithmetic average of the wall temperatures of the countercurrent vessels. θ defined by (55) is also the far field temperature that one would, for practical purposes, observe at several diameters from either vessel. Therefore, it is required that $T = \theta$ at $r = r_c$.

(iv) Axial variation of mean tissue temperature for core. Multiplying equation (41) by $(1-\beta)$ and (42) by $(1+\beta)$, adding these results, using the approximation $q_a \simeq q_v = q$, and substituting the expression for q from (52) in this last result, one can relate the variation of the mean tissue

temperature for the core or the far field temperature at r_c to the local temperature difference between the central artery and vein

$$\frac{d\theta(x,r_c)}{dx} = -\frac{\sigma_c K_t (T_a - T_v)}{\pi \rho_b c_b Q_a^2 u_a} \tag{57}$$

Equation (57) is not useful as it now stands since both T_a and T_v are unknown. A second independent relation is needed to determine the $T_a - T_v$ difference in (57). This relation can be found by considering the overall energy balance on a combined muscle-skin element that couples the heat loss at the skin surface r_s to the local losses due to blood flow and conduction at the outer edge of the core r_c as schematically shown in Figure 12. If axial conduction is neglected this energe balance can be written as

$$q_a - q_v = \pi \rho_b c_b (T_a - T_v)\frac{d(Q_a^2 u_a)}{dx} + 2\pi r_s (h_c + h_r)\left[\theta(x, r_s) - T_\infty\right] + \\ + 2\pi r_s q_{ev} - 2\pi \int_{r_c}^{r_s} q_m r\, dr \tag{58}$$

where q_m is metabolic heat production per unit volume. T_∞ is the ambient temperature and $\theta(x, r_s)$ is the unknown skin temperature. In general, $q_a - q_v$, the net conduction loss from the core, is much smaller than q_a, since radial thermal gradients at the edge of the core are small, and these small losses are well approximated by (58). A related type of imperfect countercurrent exchange occurs in the microvasculature and is fundamental to the derivation of the bioheat equation of Weinbaum and Jiji in [10].

A second relation between q_a and q_v is obtained by subtracting equation (42) from (41)

$$q_a - q_v = -\pi \rho_b c_b a_a^2 u_a \frac{d(T_a - T_v)}{dx} \tag{59}$$

Equating (58) and (59) one obtains the desired crucial relationship linking the axial variation of the temperature difference between the central artery and vein to the heat transfer processes at the skin surface

$$\frac{d(T_a - T_v)}{dx} = -\frac{T_a - T_v}{a_a^2 u_a}\frac{d(a_a^2 u_a)}{dx} - \frac{2r_s(h_c + h_r)}{\rho_b c_b a_a^2 u_a}\left[\theta(x, r_s) - T_\infty\right] - \\ - \frac{2r_s q_{ev}}{\rho_b c_b a_a^2 u_a} + \frac{2\int_0^{r_s} q_m r\, dr}{\rho_b c_b a_a^2 u_a} \tag{60}$$

Equation (57) can now be differentiated. From (48), (49) and (53) one notes that M_a and M_v are both given in terms of dimensionless length ratios that vary little with axial distance and thus σ_c can be treated as a constant. Thus equation (57) after differentiation becomes

$$\frac{d^2\theta(x, r_c)}{dx^2} = -\frac{\sigma_c K_t}{\pi \rho_b c_b}\left[\frac{1}{a_a^2 u_a}\frac{d(T_a - T_v)}{dx} - \frac{(T_a - T_v)}{a_a^4 u_a^2}\frac{d(a_a^2 u_a)}{dx}\right] \tag{61}$$

$(T_a - T_v)$ and its derivative can be eliminated in (61) using (57) and (60) and equation (40) used for $a_a^2 u_a$. After some algebraic manipulations (61) can be written as

$$\frac{d^2\theta(x, r_c)}{dx^2} - \frac{2\psi\left[\frac{\omega G^2}{\int_0^1 G^2 dz} + \frac{(1-\omega)G}{\int_0^1 G\, dz}\right]}{\psi\left[\frac{\omega_x \int_0^1 G^2 dz}{\int_0^1 G^2 dz} + \frac{(1-\omega)_x \int_0^1 G\, dz}{\int_0^1 G\, dz}\right] + (1-\psi)}\frac{d\theta(x, r_c)}{dx}$$

$$= \frac{2\sigma_c K_t}{\pi \rho_b^2 c_b^2 a_{ai}^4 u_{ai}^2 \left\{\psi\left[\frac{\omega_x \int_0^1 G^2 dz}{\int_0^1 G^2 dz} + \frac{(1-\omega)_x \int_0^1 G\, dz}{\int_0^1 G\, dz}\right] + (1-\psi)\right\}^2} \cdot \tag{62}$$

$$\cdot \left\{r_s(h_c + h_r)\left[\theta(x, r_s) - T_\infty\right] + r_s q_{ev} - \frac{q_m}{2}(r_s^2 - r_c^2)\right\}$$

Equation (62) is a basic differential equation relating

the far field temperature at the edge of the core $\theta(x, r_c)$ to the local skin temperature $\theta(x, r_s)$. The governing equation to determine $\theta(x, r_s)$ will be described next.

3.3.2 Governing Equation for Muscle Layer

Equation (62) can not be integrated unless a relation between the core temperature and the surface temperature is found. This can be obtained by applying the bioheat equation of Weinbaum and Jiji (5) in the radial direction and solving a boundary value problem for the muscle and cutaneous layers, which is similar to the model for peripheral tissue developed in Chapter 2.

An important parameter, the inflow Peclet number P_{ei} based on the conditions at the entrance to the limb,

$$P_{ei} = \frac{2\rho_b c_b a_{oi} u_{oi}}{K_b} \tag{63}$$

is defined and the bioheat equation can be written in radial coordinates. Assuming that axial conduction can be neglected and that radial derivatives of all vascular parameters are much larger than axial derivatives, this bioheat equation reduces to

$$\frac{1}{r}\frac{\partial}{\partial r}\left\{K_t\left[1 + \frac{K_b^2 a_{oi}^2 G^2}{16 K_t^2 \sigma n_o r_{ci}^2 (\int^L G^2 dz)^2}\left(\frac{n}{n_o}\right)\left(\frac{a}{a_o}\right)^4\left(\frac{u}{u_o}\right)^2 \ell_r^2 \psi^2 \omega^2 P_{ei}^2\right] r \frac{\partial\theta}{\partial r}\right\} + q_m$$

$$= \frac{K_b^2 a_{oi}^2 G^2}{16 K_t \sigma n_o r_{ci}^2 (\int^L G^2 dz)^2}\left(\frac{n}{n_o}\right)\left(\frac{a}{a_o}\right)^4\left(\frac{u}{u_o}\right)^2\left(\frac{\ell_r^2}{r} + \frac{1}{2}\frac{d\ell_r^2}{dr}\right)\psi^2\omega^2 P_{ei}^2 \frac{\partial\theta}{\partial r} \tag{64}$$

The radial variations of the coefficients of equation (64), which are related to the effective thermal conductivity, will be examined later after equation (64) is cast in non-dimensional form.

3.3.3 Governing Equation for Cutaneous Layer

In the inner region, blood reaching the cutaneous plexus from the central artery arrives at temperature θ_{bc} and undergoes an instantaneous equilibration to the local tissue temperature upon being perfused into the small vertical riser vessels emanating from this region. The strength of this distributed heat source depends on the perfusion rate and the local blood-tissue temperature difference in the cutaneous plexus

$$q_c = W_{bc}\,\rho_b\,c_b\,(\theta_{bc} - \theta) \tag{65}$$

where

$$W_{bc} = \frac{\psi(1-\omega)\,a_{ai}^2\,u_{ai}}{2\,r_{si}\,\delta_1\int^1 G\,dz} \tag{66}$$

Since this sublayer is very thin, the effect of curvature is negligible. Thus the energy equation there becomes

$$\frac{\partial^2\theta}{\partial r^2} + \frac{\psi(1-\omega)\,\rho_b\,c_b\,a_{ai}^2\,u_{ai}\,(\theta_{bc}-\theta)}{2\,K_t\,r_{si}\,\delta_1\int^1 G\,dz} = 0 \tag{67}$$

The energy equation for the outer region is simply a conduction equation since all blood vessels are in thermal equilibrium with the tissue.

$$\frac{\partial^2\theta}{\partial r^2} = 0 \tag{68}$$

3.3.4 Heat Transfer of Extremity

Because of the irregular shape and complex vascular geometry of the extremity, this research will not attempt to model the detailed blood flow and temperature field within the extremity. The overall heat loss from the extremity q_{ext}

and the volumetric blood flow rate to the extremity will be prescribed. The energy balance of the extremity provides a boundary condition for the blood temperature difference between the central artery and vein of the wrist at the entrance to the hand.

$$(T_a - T_v)_{x=L} = \frac{q_{ext}}{\pi(1-\psi)\rho_b c_b Q_{ai}^2 u_{ai}} \qquad (69)$$

The total heat loss q_{ext} due to convection, radiation and evaporation at the surface of the extremity, varies with ambient conditions. It is assumed that each surface heat transfer mechanism affects the arm and extremity in the same proportion. Thus, if the convective heat loss from the arm is doubled, so is the convective heat loss from the hand.

3.4 Dimensionless Form

3.4.1 Dimensionless Governing Equation for Each Layer

The next task is to convert the model into a coupled dimensionless boundary value problem to study the general thermal behavior of the limb and reveal the physiological significance of its crucial dimensionless parameters: ω, ψ, P_{ei}, and the three parameters that describe the surface heat loss. The following dimensionless quantities are defined:

distance in x-direction, $\tilde{x} = x/L$

distance in r-direction, $\tilde{r} = r/r_{si}$

tissue temperature, $\tilde{\theta} = (\theta - T_\infty)/(T_{ai} - T_\infty)$

central artery blood temperature, $\tilde{T}_a = (T_a - T_\infty)/(T_{ai} - T_\infty)$

central vein blood temperature, $\tilde{T}_v = (T_v - T_\infty)/(T_{ai} - T_\infty)$

cutaneous plexus blood temperature, $\tilde{\theta}_{bc} = (\theta_{bc} - T_\infty)/(T_{ai} - T_\infty)$

inflow Peclet number, $P_{ei} = 2\rho_b c_b a_{ai} u_{ai} / K_b$

metabolic heat production, $\lambda_m = q_m r_{si}^2 / K_t (T_{ai} - T_\infty)$

Biot number for convection, $B_{ic} = h_c r_{si} / K_t$

Biot number for radiation, $B_{ir} = h_r r_{si} / K_t$

evaporation heat loss, $\gamma = q_{ev} r_{si} / K_t (T_{ai} - T_\infty)$

Then the dimensionless energy equation for each region becomes

$$\frac{d^2\theta(\tilde{x},\tilde{r}_c)}{d\tilde{x}^2} - \frac{2\psi\left[\frac{\omega G^2}{\int_0^1 G^2 d\tilde{z}} + \frac{(1-\omega)G}{\int_0^1 G\, d\tilde{z}}\right]}{\psi\left[\frac{\omega_z \int_0^1 G^2 d\tilde{z}}{\int_0^1 G^2 d\tilde{z}} + \frac{(1-\omega)_z \int_0^1 G\, d\tilde{z}}{\int_0^1 G\, d\tilde{z}}\right] + (1-\psi)} \frac{d\tilde{\theta}(\tilde{x},\tilde{r}_c)}{d\tilde{x}}$$

$$= \frac{8\sigma_c K_t^2 L^2}{\pi K_b^2 Q_{ai}^2 P_{ei}^2 \left\{\psi\left[\frac{\omega_z \int_0^1 G^2 d\tilde{z}}{\int_0^1 G^2 d\tilde{z}} + \frac{(1-\omega)_z \int_0^1 G\, d\tilde{z}}{\int_0^1 G\, d\tilde{z}}\right] + (1-\psi)\right\}^2} \cdot \tag{70}$$

$$\cdot \left\{G(B_{ic} + B_{ir})\tilde{\theta}(\tilde{x},\tilde{r}_s) + G\gamma - \frac{G^2\lambda_m}{2}(1 - \tilde{r}_{ci}^2)\right\}$$

for the core,

$$\frac{1}{\tilde{r}}\frac{\partial}{\partial\tilde{r}}\left\{\left[1 + A(\tilde{r})\frac{G^2(\tilde{x})}{\left[\int_0^1 G^2(\tilde{z})\,d\tilde{z}\right]^2}\psi^2\omega^2 P_{ei}^2\right]\tilde{r}\,\frac{\partial\tilde{\theta}}{\partial\tilde{r}}\right\} + \lambda_m$$
$$= B(\tilde{r})\frac{G^2(\tilde{x})}{\left[\int_0^1 G^2(\tilde{z})\,d\tilde{z}\right]^2}\psi^2\omega^2 P_{ei}^2\frac{\partial\tilde{\theta}}{\partial\tilde{r}} \tag{71}$$

for the muscle,

$$\frac{\partial^2\tilde{\theta}}{\partial\tilde{r}^2} + \frac{\psi(1-\omega)K_b Q_{ai} r_{si}}{4K_t \delta_1 L \int_0^1 G(\tilde{z})\,d\tilde{z}} P_{ei}(\tilde{\theta}_{bc} - \tilde{\theta}) = 0 \tag{72}$$

for the inner cutaneous layer,

$$\frac{\partial^2\tilde{\theta}}{\partial\tilde{r}^2} = 0 \tag{73}$$

for the outer cutaneous layer, where

$$A(\tilde{r}) = \frac{K_b^2 Q_{ai}^2}{16K_t^2 \sigma n_0 r_{ci}^2 L^2}\left(\frac{n}{n_0}\right)\left(\frac{Q}{Q_0}\right)^4\left(\frac{U}{U_0}\right)^2 \ell_r^2 \tag{74}$$

and

$$B(\tilde{r}) = \frac{K_b^2 a_{ai}^2}{16 K_t^2 \sigma n_0 r_{ci}^2 L^2} \left(\frac{n}{n_0}\right)\left(\frac{a}{a_0}\right)^4 \left(\frac{u}{u_0}\right)^2 \left(\frac{\ell_r^2}{\tilde{r}} + \frac{1}{2}\frac{d\ell_r^2}{d\tilde{r}}\right) \qquad (75)$$

3.4.2 Functions $A(\tilde{r})$ and $B(\tilde{r})$

The functions $A(\tilde{r})$ and $B(\tilde{r})$ defined by (74) and (75) describe the radial variation of the microvascular geometry of the countercurrent vessels as one proceeds from the central artery and vein towards the skin surface. These functions involve products of either properties of tissue and blood, functions of geometry varying with tissue depth and the dimensionless velocity ratio u/u_0. If uniform blood perfusion in the muscle layer is assumed, one can show that the ratio u/u_0 can be calculated from the conservation of fluid mass and depends on the vascular geometry only (see Chapter 2 for details). Convenient functional forms for the variation of the vascular geometry of the muscle layer in the radial direction have been proposed in Chapter 2. These forms are

$$a/a_0 = (d_1 + d_2\tilde{r})^{d_3} \qquad (76)$$

$$n/n_0 = (d_4 + d_5\tilde{r})^{d_6} \qquad (77)$$

$$\sigma = \frac{\pi}{\cosh^{-1}(d_7 + d_8\tilde{r}^{d_9})} \qquad (78)$$

$$\ell_r = \cos(d_{10} + d_{11}\tilde{r}) \qquad (79)$$

The quantities $\ell_r =$ ... d_1 to d_{11}, a_0 and n_0 are listed in Table 3. They are based on approximate measurements obtained from vascular casts of muscle tissue in the rabbit thigh [7]. The diminution in vessel size with branching should be

independent of species. This variation of the vascular parameters with depth in the muscle layer is summarized in Table 4.

3.4.3 Effective Thermal Conductivity of Muscle Tissue Layer

The term in square brackets on the left hand side of equation (71) represents the ratio of effective blood-tissue conductivity in the radial direction in the muscle tissue layer to the conductivity of non-perfused tissue

$$\frac{K_{eff}}{K_t} = 1 + A(\tilde{r})\left[\frac{G^2(\tilde{x})}{\left[\int_0^1 G^2(\tilde{z})\,d\tilde{z}\right]^2}\psi^2\omega^2 P_{ei}^2\right] \qquad (80)$$

The enhancement of conductivity is due to two factors: the variation of vascular geometry in the radial direction $A(\tilde{r})$ and the local Peclet number describing the bleed-off from the central artery to the muscle layer $G(\tilde{x})\psi\omega P_{ei} / \int_0^1 G^2\,d\tilde{z}$. Thus, the effective conductivity varies with radial distance as well as axial distance when the cross-sectional area of the arm changes in axial direction, i.e., $G \neq 1$. In Figure 13 the variation of effective conductivity at the entrance of a tapered arm is examined. It is observed that the effective conductivity decreases rapidly towards its conduction value as vessel size decreases below 100 μm and the greatest enhancement which is a factor of 4 or more occurs near the core. This allows heat generated in the deep portion of the muscle layer, which is far removed from the cutaneous circulation, to be transferred efficiently. A second important observation is that the effective conductivity is proportional to the square of the local Peclet number and

thus the blood flow rate provides a non-linear enhancement of the effective conductivity. Therefore, a large enhancement is possible during exercise to promote the removal of heat from the core of the limb. Both these features, which are dependent on the branching countercurrent structure of the microvasculature, were previously unrecognized.

3.4.4 Dimensionless Metabolic Heat Production

The dimensionless metabolic heat production λ_m in equation (71) is only important in the muscle layer. Because metabolic heat production is directly proportional to the oxygen consumption, and the oxygen uptake is related to the blood flow rate in this region, the dimensionless metabolic heat production and the blood supply to the muscle layer are coupled and a simple linear relationship between them can be assumed. Thus,

$$\lambda_m = d_{12}\Psi\omega P_{ei} + d_{13} \qquad (81)$$

where constants d_{12} and d_{13} are determined by evaluating (81) at any two known conditions. If one uses as the two representative cases, the value $\lambda_m = 0.215$ for the supine resting state, and $\lambda_m = 2.15$ for moderate exercise, d_{12} and d_{13} are found to be 0.00026 and -0.43, respectively. This corresponds to P_{ei} = 3500 in the resting state and P_{ei} = 14000 during moderate exercise.

3.4.5 Dimensionless Blood Temperature of Cutaneous Plexus

$\tilde{\theta}_{bc}$ in (72) stands for the dimensionless temperature of the blood from the central artery when it arrives at the

cutaneous plexus. $\tilde{\theta}_{bc}$ depends on the prior equilibration in the large isolated riser vessels and is thus related to the blood flow rate into the cutaneous layer. In the supine resting state in a cool environment, when this flow is very slow, blood entering the cutaneous plexus will have equilibrated to the local tissue temperature. In this limit, $\tilde{\theta}_{bc}$ is equal to the dimensionless local tissue temperature that would be obtained at the base of the cutaneous layer if there were no blood perfusion in this layer. In the other limit, maximum vasodilation, The flow rate to the cutaneous layer is so large that there is little thermal equilibration of the blood before it enters the cutaneous layer. In this limit, the dimensionless blood temperature $\tilde{\theta}_{bc}$ is equal to that of the central artery at the same axial location, i.e., $\tilde{\theta}_{bc} = \tilde{T}_a$. If one assumes a simple linear relationship between the ratio of $\tilde{\theta}_{bc}$ to $\tilde{T}_a$ and the blood flow rate to the cutaneous layer

$$\tilde{\theta}_{bc} / \tilde{T}_a = d_{14} \psi (1-\omega) P_{ei} + d_{15} \qquad (82)$$

The constant d_{15} depends on the local temperature profile when $\omega \simeq 1$ and is therefore related to the solution of (71) and (72) in the supine resting state for a given set of environmental conditions. d_{14} is then determined for conditions of maximum flow. Both d_{14} and d_{15} are listed in Table 3.

3.5 Six Key Parameters

Six independent dimensionless parameters enter in the

mathematical model, the inflow Peclet number P_{ei} at the entrance of the central artery, the ratio ψ of the blood supply to the arm to the total blood supply to the limb, the ratio ω of the blood supply to the muscle layer to the total blood supply to the arm, the convective Biot number B_{ic}, the radiative Biot number B_{ir}, and the dimensionless evaporation heat loss γ. The former three parameters describe the body conditions (internal parameters) while the later describe the surrounding conditions (external parameters).

The inflow Peclet number is mostly affected by the level of exercise. The blood velocity of the central artery at the entrance to the limb varies approximately from 7.5 cm/sec to 30 cm/sec, which corresponds to the range of inflow Peclet numbers from 3500 to 14000.

The distribution of blood supply between the arm and extremity does not vary significantly with the level of exercise except for the case where the arm and extremity are placed in two different climate-controlled chambers for research purposes. Under normal conditions, ψ is taken to be a constant whose value is 0.75.

It is well known that the control of the cutaneous blood flow is the major thermoregulatory effector process. In the supine resting state and a neutral environment the cutaneous layer is vasoconstricted. Most of the blood circulates in the muscle tissue with a representative value for ω being approximately 0.97. During conditions of maximum vasodilation of the cutaneous vessels, the cutaneous

circulation can be increased more than 15 times. This corresponds to an ω of approximately 0.5.

Heat is transferred from the surface of the arm by convection (free or forced), radiation and evaporation. The convective heat flux at the surface is

$$(q/A)_c = h_c(T_s - T_\infty) \tag{83}$$

Using the correlation equation in [18], h_c is found to be about 3.5 W/m^2-°C for free convection. The corresponding convective Biot number is 0.49 and this value can be increased by a factor of 10 for forced convection with a free stream velocity of about 10 MPH.

All objects continually radiate energy in accordance with the Stefan-Boltzmann law. The radiative heat flux on the surface is

$$\begin{aligned}(q/A)_r &= \epsilon\sigma(T_s^4 - T_\infty^4) \\ &= \left[\epsilon\sigma(T_s^3 + T_s^2 T_\infty + T_s T_\infty^2 + T_\infty^3)\right](T_s - T_\infty)\end{aligned} \tag{84}$$

Note that the term in the square brackets is almost constant because an absolute temperature scale must be used. This term can be defined as a radiative heat transfer coefficient h_r which is about 7 W/m^2-°C, when one uses the recommended empirical equation in [24]. Thus the radiative heat transfer has the same form as the convective heat transfer except h_c is replaced by h_r in equation (83). The corresponding radiative Biot number is calculated to be 0.98 and remains about the same under most physiological conditions.

Water diffusion through the human skin is part of the

"insensible" perspiration which is not subject to thermo-regulatory control. This diffusion totals about 350 ml/day in an average person and is assumed to be proportional to the difference between the vapor pressure of water at the skin temperature and the partial pressure of water vapor in the ambient air. Under normal conditions the average heat loss by this mechanism is about 5.2 W/m^2 which corresponds to a dimensionless evaporation heat loss γ of 0.0485. However, when activity level of tne body rise above the basal state, the need to reject more heat from the body arises. An autonomic mechanism for increasing the heat loss, the sweating response, results in a significant increase in γ. The maximum value for γ is more than 10 times larger than that of the basal state.

3.6 Boundary Value Problem for Whole Limb and Solution Procedure

In order to solve this complicated boundary value problem, all the known and unknown variables of the model are listed below:

(i) prescribed parameters

(a) ω, ψ and P_{ei} describe the blood flow rate to limb and its distribution;

(b) B_{ic}, B_{ir} and γ describe the heat transfer at the skin surface;

(c) $G(\tilde{x})$ describes the axial variation of the local radius of the arm.

(ii) prescribed boundary conditions

(a) $\tilde{T}_a(0)$ is the arterial blood temperature at the entrance to the limb;

(b) $\tilde{T}_a(1) - \tilde{T}_v(1)$ is the blood temperature difference between the central artery and vein at the wrist and is given by equation (69).

(iii) unknown boundary conditions

(a) $\tilde{T}_v(0)$ is the blood return temperature in the central vein at the entrance to the limb;

(b) $\tilde{T}_a(1)$ or $\tilde{T}_v(1)$ is the blood temperature in the the central artery or vein at the wrist;

(c) $\tilde{\theta}(\tilde{x},\tilde{r}_s)$ is the surface temperature of the arm.

(iv) unknown field variables

(a) $\tilde{T}_a(\tilde{x})$ and $\tilde{T}_v(\tilde{x})$ are the blood temperatures in the central artery and vein;

(b) $\tilde{\theta}(\tilde{x},\tilde{r})$ is the tissue temperature within the arm.

The energy equations for the core, muscle and cutaneous layers are coupled and must be solved by numerical methods. The arm is first descretized into disk like elements in the axial direction by planes perpendicular to its axis. Each element contains the central part of the core surrounded by two annular rings of the muscle and cutaneous layers. The arterial blood temperature $\tilde{T}_a(0)$ when it enters the first element is known but the venous return temperature $\tilde{T}_v(0)$ when the blood leaves the limb is unknown. This temperature is guessed to start the solution procedure. Using these entrance and exit temperatures of the central vessels, one

calculates the mean tissue temperature of the core, or the tissue temperature at the edge of the core $\tilde{\theta}$ for the first element using equation (55). This mean tissue temperature of the core then serves as a boundary condition for the muscle layer at the interface between the core and muscle layer in the initial element. The governing equations (71), (72) and (73) for the muscle layer, the inner and outer regions of the cutaneous layer are then integrated numerically in radial direction to find the temperature distribution within this element. In proceeding from one layer to another, the tissue temperature and heat flux at the interface must be matched. This matching determines the surface temperature of the initial element. Using the surface temperature of the first element found in this manner, one next integrates the energy equation for the core (70) numerically in the axial direction to find the temperatures of the core tissue, the central arterial and venous blood in the second element. Alternately applying the governing equations in the radial and axial directions, one can repeat the entire procedure and in this manner determine the temperature field throughout the entire arm, including the central arterial and venous blood temperatures in the last element, $\tilde{T}_a(1)$ and $\tilde{T}_v(1)$. The boundary condition at the end of the arm, $\tilde{T}_a(1)-\tilde{T}_v(1)$, is then used as an end point constraint to determine the correct value of the guessed temperature $\tilde{T}_v(0)$. The whole procedure is repeated until a correct $\tilde{T}_v(0)$ is found and the temperature field of the arm corresponding to that $\tilde{T}_v(0)$ is obtained.

3.7 Results and Discussion

Sample calculations to illustrate the application of the model have been presented in [25] for the simplest case, G=1 or an arm of constant cross-sectional area. The results for a more realistic case, a tapered arm where the radius of the arm at its entrance is twice as large as that at its end, or $G = 1-\tilde{x}/2$, are presented herein.

Figures 14, 16, 18 and 19 show the axial variation of the central artery, vein and skin surface temperatures and Figures 15, 17 and 20 are the corresponding results for the radial temperature profiles. In general, the dimensional radial gradients in the muscle tissue are about two orders of magnitude larger than the axial gradients and thus the neglect of axial conduction is well justified.

Figures 14, 16 and 18 show how the central artery and vein function as an imperfect countercurrent heat exchanger. There is a net loss of heat from the central artery and vein to the muscle and cutaneous layers by conduction and convection (radial bleed-off to the microcirculation of both these layers) as shown in Figure 12. The net conductive heat transfer (q_a-q_v), is governed by equation (59) which shows that it is proportional to the axial gradient of the temperature difference between the central artery and vein. The convective heat transfer, on the other hand, is equal to $(P_m+P_s)\rho_b c_b (T_a-T_v)$ and thus proportional to the temperature difference of the central artery and vein. The relative importance of each transfer mechanism depends on the blood

flow distribution and external conditions and will be analyzed for different cases. The quantity $(q_a-q_v)/q$, which represents the ratio of conductive heat loss from the core to the surrounding tissue to the heat exchange between the central artery and vein if they were to function as a perfect countercurrent heat exchanger ($q=q_a=q_v$), is found to vary in the axial direction with minimum and maximum values that fall between 12 % and 35 % for most physiological conditions. This means that about 65 to 90 percent of the conductive heat transfer takes place between the countercurrent vessel pair while the rest occurs between the vessel pair and surrounding tissue. The assumption that q_a or q_v individually is larger than their difference (q_a-q_v) thus appears to be a reasonable approximation even for the large central vessels.

The next step is to examine the thermal behavior of the limb under different physiological and environmental conditions by varying one parameter while holding the others fixed.

Figure 14 shows the variation of the dimensionless temperature of the central artery, vein and skin surface in the axial direction for different blood flow rates to the entire limb described by the inlet flow parameter P_{ei}. In general, the level of P_{ei} indicates the state of exercise or the oxygen demand of the muscle tissue. Higher temperatures of the central artery, vein and surface result from a higher blood flow rate and thus a higher metabolic heat production rate. Note that the temperature difference between the

central artery and vein would remain constant even if there were radial bleed-off if the countercurrent heat exchange were perfect and no heat were conducted out of the core to the muscle tissue. The temperature difference of the central artery and vein and its gradient are both small at high blood inflow rates. Two factors contribute to this behavior: (1) at high flow rates the countercurrent conductive exchange is reduced and (2) more metabolic heat is generated in the muscle layer which reduces the radial temperature gradient in the central region of the limb and hence the heat flux in this region. Thus, both the conductive and convective heat transfer from the central vessel pair to the surrounding tissue are low. For these conditions, one can show that the central artery and vein behave as a nearly perfect counter-current heat exchanger, and the temperature difference between them $(\tilde{T}_a - \tilde{T}_v)$ is small. Although not shown in Figure 14 it is possible under conditions of maximum exercise, when the blood flow rate and metabolic heat production are high enough, for the blood in the central artery to become sufficiently heated for its temperature to exceed that at the entrance to the limb, i.e., $\tilde{T}_a > 1$. It is observed that the skin surface temperature decreases more rapidly in the axial direction than the central artery and vein temperatures. This is believed to be attributable to the tapered geometry of the arm. A smaller local cross-sectional area of the muscle layer, which is equivalent to smaller local blood perfusion and metabolic heat generation rates, leads to a

lower surface temperature there.

Since the central vessel and skin surface temperatures vary in the axial direction for a tapered arm, to show the radial temperature profiles, an axial position should be specified. The dimensionless radial temperature profiles at $\tilde{x} = 0.05$, which is near the entrance of the arm, are shown in Figure 15 for the same conditions as Figure 14. These profiles are flat in the deep portion of the muscle layer because of the enhancement in conductivity in this region due to countercurrent microvascular heat exchange, see Figure 13. This effect is particularly evident at high flow rates. It is also observed that at the higher blood flow rates the temperature of the tissue is elevated throughout the arm. The latter effect can be shown to be due to increased metabolic heat production resulting from the increased oxygen consumption of the muscle tissue. To show this consider an imaginary situation where P_{ei} and λ_m are not coupled by equation (81). Thus suppose $P_{ei} = 14000$ but λ_m is assigned a value that corresponds to $P_{ei} = 7000$. The resulting curve is the dashed line in Figure 15. This curve lies between the solid curves for $P_{ei} = 7000$ and $P_{ei} = 14000$ where blood flow rate is coupled with metabolic heat production, and thus shows that both effects contribute to the increase of the tissue temperature.

The importance of the cutaneous circulation in whole limb heat transfer can be easily seen in Figure 16, which shows how the axial temperature profiles of the central

artery, vein and skin surface are altered by increasing the fractional blood supply to the cutaneous layer. Decreasing ω and hence increasing the proportion of the total blood supply to the cutaneous circulation, i.e., more warm blood is pumped from the center to the surface to be cooled, leads to a decrease in temperature of the central vessels but an increase in skin surface temperature. More heat is transferred at the surface. This would occur when the body needs to reject its internal heat. The opposite is also true when the body wants to conserve heat in a cold environment. This effect of the cutaneous circulation can be more easily understood with the aid of Figure 17 which shows the temperature profiles in the radial direction at $\tilde{x} = 0.05$. Dilating the cutaneous circulation lowers the core tissue temperature but elevates the skin surface temperature since warm blood from the core is brought to the inner region of the cutaneous layer. One should also compare the inset figures I and II showing the detailed temperature distribution near the skin surface for low and high values of ω. The temperature gradient changes significantly across the cutaneous layer for the case of low ω. The magnitude of the gradient at the skin surface is approximately twice as large as its value at the interface between the muscle and cutaneous layers, and is also larger than its value at the skin surface for the case of large ω. This rapid change in gradient makes it possible to transfer more heat to the surroundings and thus reduce the temperature throughout

the limb.

Figures 18, 19, and 20 show the dimensionless axial temperatures of the central artery, vein and skin surface, and the tissue temperature profiles in radial direction at $\tilde{x} = 0.05$, respectively, when the convective heat transfer at the surface is increased from values typical of natural convection to forced convection with a high wind speed. This surface cooling decreases the temperature of the arm throughout but the decrease in surface temperature is more pronounced. Also the inset figure in Figure 20 shows that for a high convective heat transfer coefficient, the temperature gradient at the surface becomes steeper. This occurs because the strength of the thermal source term in the inner skin layer increases in proportion to the $(\theta_{bc} - \theta)$ difference as the skin is cooled.

Figures for different values of B_{ir} and γ can be obtained in a similar way but these are unnecessary since radiative and evaporative heat transfer at the surface play the same role as convective heat transfer and plots similar in character to Figures 18, 19 and 20 would be obtained.

3.8 Comparison between Theoretical Predictions and Experimental Measurements and Future Improvements of Model

In Pennes experiments [1] a small stainless steel needle was inserted into the forearm of a normotensive male subject who was lying on a bed in a climate-controlled room. A Y-model thermocouple was then traversely passed through the arm. Temperature measurements were taken while the depth of

the thermocouple below the skin was regulated and measured by a wire-controller. This experiment was performed on a total of 9 subjects. A representative traverse temperature profile of the the human forearm based on the mean experimental data of all these subjects was plotted in Figure 16 in [1] and is shown as the dash-dot curve in Figure 21. The maximum temperature does not occur at the axis of the arm because of the asymmetry of the central vessels. The dashed curves are the theoretically predicted temperature profiles obtained from the solution of the Pennes bioheat equation for several representative blood perfusion rates V. While there is a rough qualitative agreement between those curves and the experimental profile, the theoretical curves based on the Pennes bioheat equation are much fuller and have the wrong slope near the skin. This error in shape is due to the blood perfusion source term in Pennes bioheat equation. According to the new bioheat equation subcutaneous regions near the skin surface where the microvessels are less than 50 μm should show little enhancement in conductivity since thermal equilibrium between the vessels and the tissue is virtually complete. Thus, the heat source term due to blood perfusion in this region should vanish. The solid curves in Figure 21 are the theoretically predicted temperature profiles using the bioheat equation of Weinbaum and Jiji for a subject in a supine resting state and thermoneutral environment according to different correlation equations for the heat transfer at the skin surface. Solid curve I is obtained when the convective heat transfer coefficient h_c is taken from the earlier

correlation equation that Pennes used in his model and the radiative heat transfer is neglected while in solid curve II the radiative heat transfer is considered. The convective and radiative heat transfer coefficients h_c and h_r for solid curve III are calculated from the correlation equations in [18], which are believed to be more superior than those obtained 40 years ago. Thus this curve gives a more accurate prediction of temperature profile under the experimental conditions. It is important to realize that there are no fudge factors or free parameters in the new bioheat equation since all vascular parameters have been prescribed and there is no attempt to curve fit the experimental data. The agreement between the theoretical prediction and the experimental measured radial temperature profile is extraordinary. For supine resting conditions, the enhancement of the conductivity and metabolic heat generation of the tissue are small. The fact that conduction dominates the tissue heat transfer over the entire peripheral tissue region is confirmed by the nearly linear temperature profiles in this region in both the theoretical predictions of the new bioheat equation and the experimental measurements. The theoretical curve has a flat temperature distribution near the axis of the arm arising from the model assumption that the central region of the arm is treated as a core with a uniform mean temperature obtained by integrating the tissue temperature over the cross-sectional area of the core. The small deviation of the theoretical temperature profile from the experimental one

could be made to vanish by introducing small changes in the assumed functional forms that represent the actual microvascular organization and adding the effect of the bone. Although more experiments should be conducted in other physiological conditions in the future to further verify this model, it seems reasonable that the new theoretical model provides for a much more accurate prediction of the thermal behavior of the whole limb than any previous models.

Improvements are obviously needed in the future modeling of whole limb heat transfer to take into account the three-dimensionality arising from the asymmetry of the central vessels and the bifurcation of these vessels when they enter the lower limb. However, the principal bifurcation leads to two major countercurrent vessel pairs which are on opposite aspects of the limb and thus do not interact strongly. A reasonable straightforward approach is to construct at each axial station an equivalent axisymmetric geometry where the radial heat transfer is approximately the same as for the actual asymmetric vessel configuration. Assuming an average effective conductivity for the entire cross-section, the bicircular transformation can be used to calculate the approximate increase in heat flux from an eccentrically located core of radius r_c to an outer cylinder of radius r_s. This increase in radial heat flux can then be accounted for by either modifying the average effective conductivity or increasing the radius of the core for the locally equivalent axisymmetric model. The effect of vessel bifurcation would

be treated by simply adding the radial heat transfer from each vessel pair.

It is also well recognized that the geometry and vasculature of the extremity make it an extremely important heat transfer organ. Raman and Vanhuyse in a series of papers (26-28) provided the first detailed quantitative experimental and theoretical studies exploring the relative importance of the deep tissue and cutaneous circulations in the human hand. Their experiments which measured the total blood flow to and heat loss from the hand when immersed in a stirred water bath showed that the steady state heat loss decreased linearly when the bath temperature was varied from 40°C to 25°C, but that between 25°C and 10°C a transition in behavior occurred which resulted in a minimum heat transfer at about 13°C. To describe this behavior, their model allowed for two rather than a single venous return path from the central artery, a superficial vein which did not undergo countercurrent heat exchange and a deep countercurrent vein which did. If the bath temperature was lowered, a sufficient shunting of blood from the cutaneous to the deep vein occurred and a minimum heat loss could be accounted in their model. This superficial vein originates in the extremity and then runs the length of the arm just beneath the cutaneous layer. The effect of large subcutaneous veins in whole limb heat transfer is therefore probably significant and should be added in future refinements of the present model.

Further verification of this whole limb heat transfer

model under different physiological conditions is necessary. This requires experimental studies where all important input parameters can be directly or indirectly measured and critical temperature and heat flux measurements made to test theoretical predictions. The experiments can be carried out in stages. The first stage may entail the quantification of the following under steady state thermoneutral conditions in the human forearm: hand heat loss and blood flow, average axial surface temperature distribution of the arm and the distribution of blood flow between the muscle tissue and cutaneous circulations of the arm. These can be obtained by using the thermocouple probes in [11] for temperature measurements, and an environmental chamber with a plethysmograph-calorimeter for blood flow and heat loss measurements. The latter is similar to that used in [26]. In a separate set of experiments K_{eff} can be determined in the rabbit thigh as a function of tissue depth so that invasive measurements on human subjects will be avoided. These experiments will produce the data necessary to verify the model for heat transfer in the arm under thermoneutral conditions. In the later stages, experiments can be conducted to explore how the partitioning of the blood flow between skin and muscle and between arm and hand is affected by other physiological conditions rather than the thermoneutral one. Also precise measurements for hand heat transfer will reveal its thermoregulatory control.

4. Conclusion

This theoretical model of peripheral tissue and whole limb heat transfer based on the bioheat equation of Weinbaum and Jiji has set a stage for a new generation of bioheat transfer models. Unlike those previously proposed models in which the vascular geometry was neglected and only the overall effect of blood flow on tissue heat transfer was considered, this model takes into account the local enhancement of heat transfer due to the local vascular organization. By applying the new bioheat equation, the contributions of the vascular geometry and the blood flow on heat transfer can be separated. Once the vasculature of a specific tissue organization is known from anatomy, the new bioheat equation can be integrated with little difficulties to provide an accurate prediction of the temperature field and surface heat transfer rate under a wide range of physiological conditions. This model also provide a better understanding of the fundamental mechanisms of macro- and micro-vascular heat transfer and their coupling by showing how the heat exchange from the large countercurrent central vessels can be matched to the microvascular heat exchange of the surrounding muscle tissue. This is an important conceptual question that has not been previously examined.

The new model can be further developed and used in a wide variety of applications. For example, in the study of a tissue freezing process in a cryosurgical procedure, the new bioheat equation governs the unfrozen region while a pure

conduction equation describes the frozen region. With the phase transformation condition at the interface between them, the transient solution provides the advance velocity of the ice front at each moment and the steady state solution gives the final size of the cryogenic lesion.

Similar models can be constructed for torso and head with internal heat sources from the active organs (e.g., liver, heart and brain) added into them. When they are combined with the model of limb heat transfer, a complicated model for whole body heat transfer is formed which should include the interaction between the body and the environment, between parts of the body, and between layers in each part. Therefore, in conclusion the new model for whole limb heat transfer developed herein appears to lay the foundation for a new generation of steady and unsteady whole body models in which vascular organization and flow can be related to whole body thermoregulatory function.

Table 1

Model Properties and Constants

a_o = 150 μm	C_1 = 0.823
L_1 = 2 cm	C_2 = 2
L_2 = 0.3 cm	C_3 = 0.933
L_3 = 0.1 cm	C_4 = 0.7
L_4 = 0.1 cm	C_5 = 1.2
S_{DI} = 2.5444 cm	C_6 = 4.75
ρ_b = 1.05 g/cm^3	C_7 = 16
c_b = 3.8 x 10^3 J/kg-°C	C_8 = 0.7854
k_b = k_t = 0.5 W/m-°C	

Table 2

Variation of Vascular Variables and Effective Conductivity in Deep Tissue Layer

$\tilde{z}_1$	n #pairs/cm^2	a cm	σ	ℓ_1	A ($\tilde{z}_1$)	B ($\tilde{z}_1$)	u cm/sec (Pe_o=60)	$\frac{k_{eff}}{k_t}$	u cm/sec (Pe_o=120)	$\frac{k_{eff}}{k_t}$	u cm/sec (Pe_o=240)	$\frac{k_{eff}}{k_t}$
0	1	0.01500	4.532	0.7071	0.0000612	0.0000481	2.5	1.220	5	1.878	10	4.512
0.1	1.187	0.01400	4.532	0.7604	0.0000497	0.0000334	2.205	1.178	4.41	1.711	8.82	3.844
0.2	1.433	0.01298	4.532	0.8090	0.0000382	0.0000218	1.925	1.137	3.85	1.547	7.7	3.188
0.3	1.763	0.01192	4.532	0.8526	0.0000276	0.0000133	1.66	1.099	3.32	1.395	6.64	2.580
0.4	2.222	0.01081	4.532	0.8910	0.0000186	0.0000074	1.413	1.067	2.825	1.267	5.65	2.068
0.5	2.887	0.00966	4.532	0.9239	0.0000116	0.0000038	1.18	1.042	2.36	1.166	4.72	1.664
0.6	3.903	0.00844	4.524	0.9511	0.0000071	0.0000018	0.968	1.023	1.935	1.093	3.87	1.372
0.7	5.565	0.00714	4.399	0.9724	0.0000033	0.0000006	0.775	1.012	1.55	1.047	3.1	1.188
0.8	8.570	0.00573	3.694	0.9877	0.0000016	0.0000002	0.608	1.006	1.215	1.023	2.43	1.092
0.9	14.873	0.00416	2.262	0.9969	0.0000008	0.00000005	0.475	1.003	0.95	1.011	1.9	1.044
1.0	32	0.00225	1.268	1	0.0000002	0	0.455	1.001	0.91	1.003	1.81	1.012

Table 5

Model Properties and Constants

$L = 70$ cm

$r_{si} = 7$ cm

$r_{ci} = 2$ cm

$\delta_1 = \delta_2 = 0.1$ cm

$a_{ai} = 0.3$ cm

$a_o = 0.05$ cm

$n_o = 0.14$ pair/cm^2

$\rho_b = 1.05$ g/cm^3

$c_b = 3800$ J/kg-°c

$K_b = K_t = 0.5$ W/m-°c

$d_1 = 1.372$

$d_2 = -1.301$

$d_3 = 1.4$

$d_4 = 1.408$

$d_5 = -1.429$

$d_6 = -1.4$

$d_7 = 1.25$

$d_8 = 15.4$

$d_9 = 40$

$d_{10} = 1.484$

$d_{11} = -1.528$

$d_{12} = 2.6 \times 10^{-4}$

$d_{13} = -0.43$

$d_{14} = 9.5 \times 10^{-5}$

$d_{15} = 0.502$

Table 4

Variation of Vascular Variables in Muscle Layer at the Entrance of the Limb

$\tilde{r}$	a cm	n # pairs/cm^2	σ	ℓ_r	$A(\tilde{r})$	$B(\tilde{r})$
0.286	0.0500	0.140	4.532	0.500	1.13×10^{-7}	6.95×10^{-7}
0.354	0.0439	0.162	4.532	0.588	7.96×10^{-8}	3.92×10^{-7}
0.423	0.0380	0.190	4.532	0.669	5.37×10^{-8}	2.18×10^{-7}
0.491	0.0324	0.228	4.532	0.743	3.46×10^{-8}	1.18×10^{-7}
0.560	0.0270	0.281	4.532	0.809	2.06×10^{-8}	5.95×10^{-8}
0.629	0.0219	0.360	4.532	0.866	1.10×10^{-8}	2.72×10^{-8}
0.697	0.0171	0.484	4.532	0.914	5.18×10^{-9}	1.10×10^{-8}
0.766	0.0127	0.711	4.532	0.951	1.92×10^{-9}	3.45×10^{-9}
0.834	0.0087	1.195	4.448	0.978	5.01×10^{-10}	7.63×10^{-10}
0.903	0.0052	2.800	3.234	0.995	6.90×10^{-11}	8.76×10^{-11}
0.971	0.0023	32.00	1.268	1	1.54×10^{-17}	1.58×10^{-17}

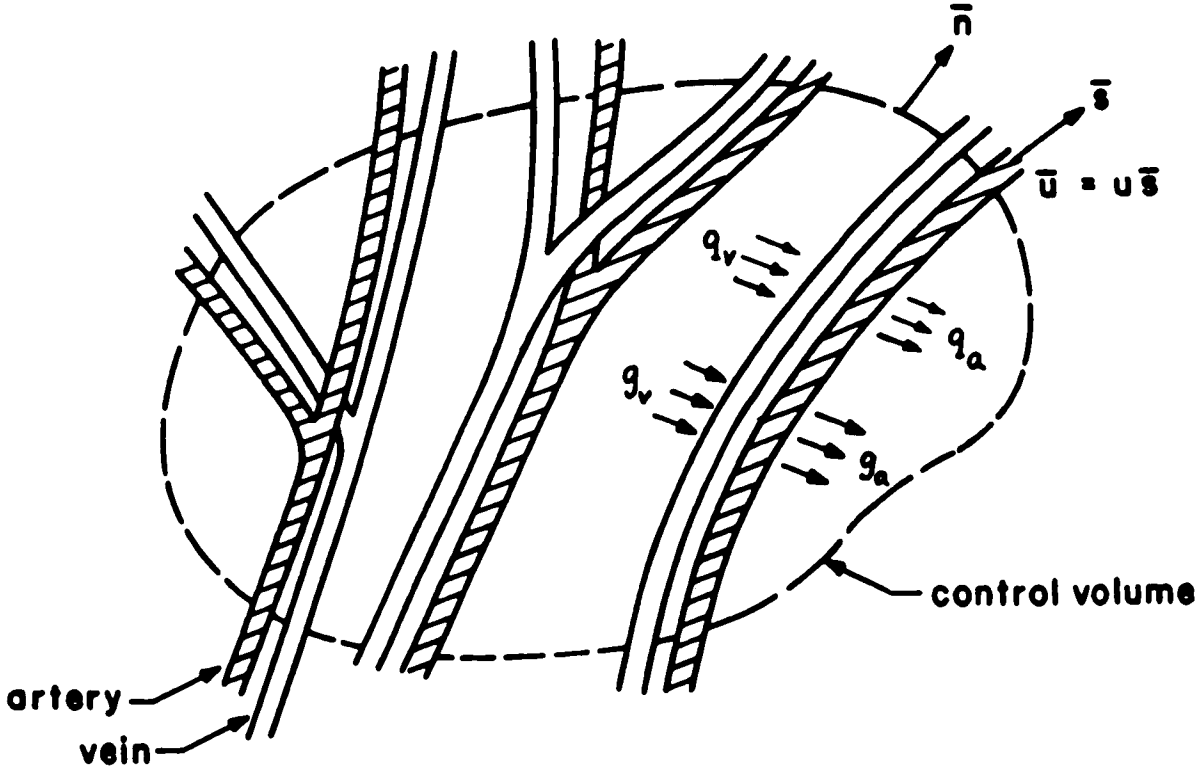

Fig.1 Control volume

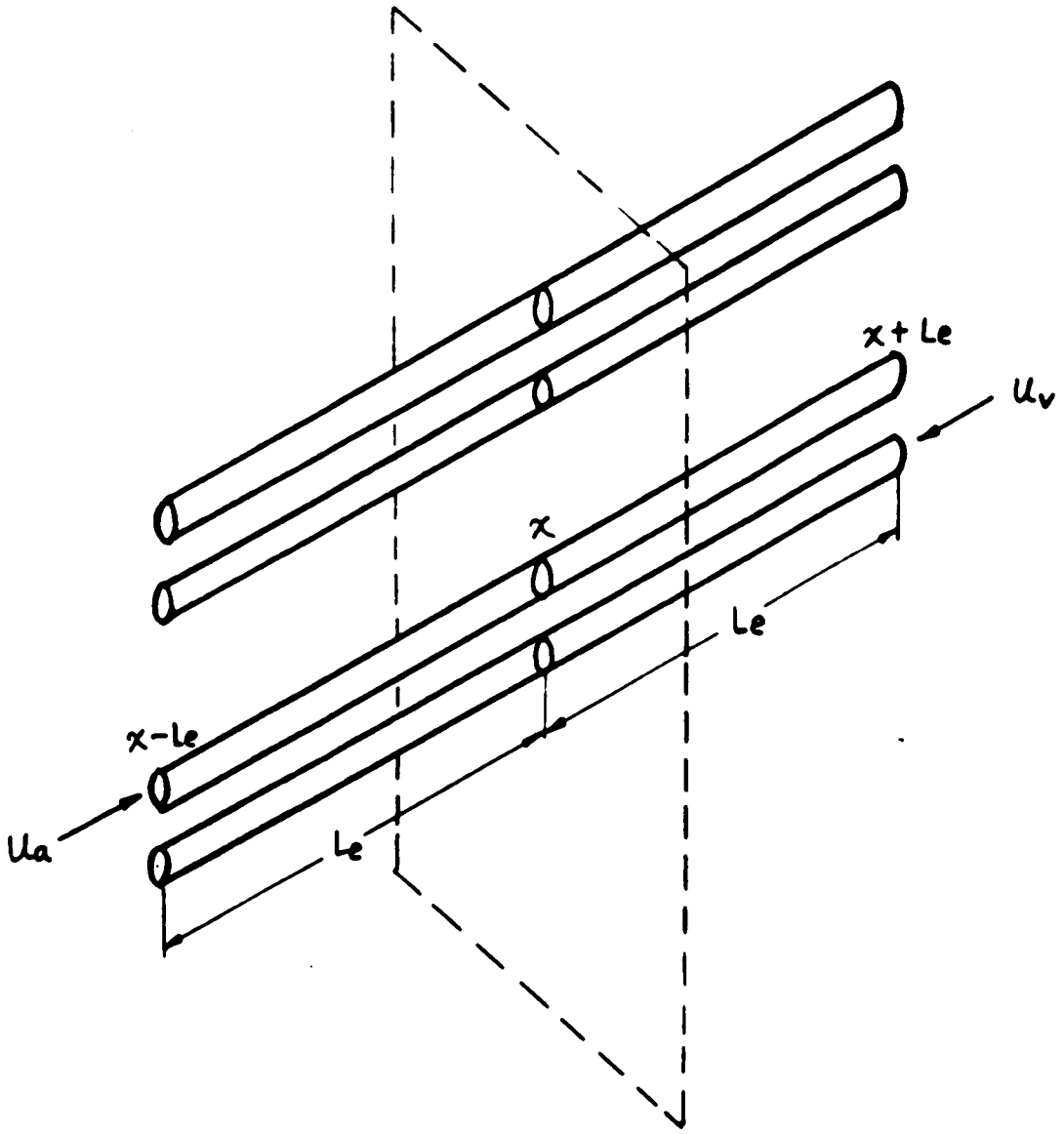

Fig.2 Countercurrent heat flux enhancement

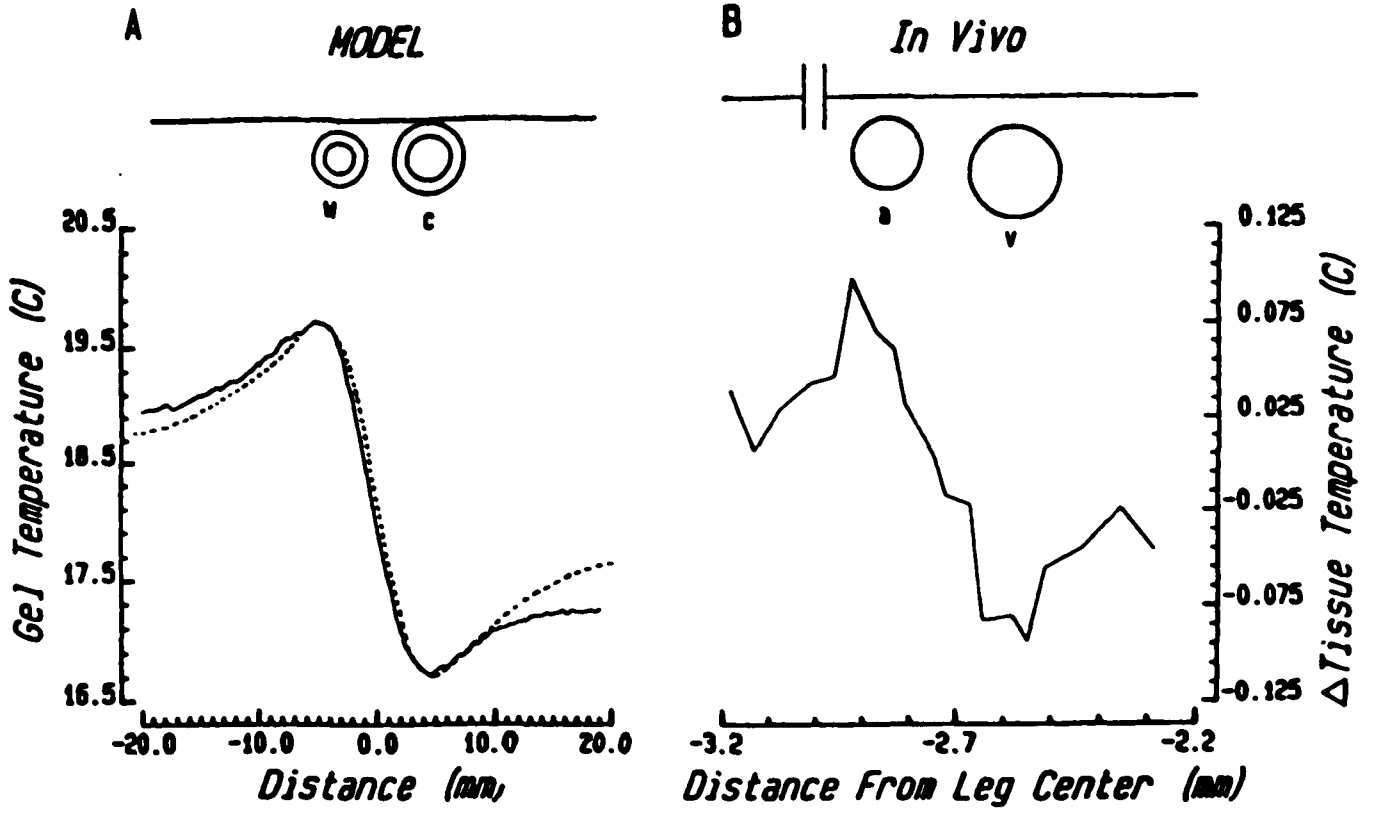

Flg.3 Model and in vivo temperature measurements. Panel A: Temperature profile for thermal couple traverse through gelatin block with countercurrent tube flow. Dimensions of tubes and location of wire shown in upper part of diagram scaled relative to dimensions of vessels and position of wire for in vivo traverse shown in Panel B. Solid curve is experimentally measured profile, dashed curve is theoretically predicted profile using bicircular conduction solution with uniform wall temperatures. Panel B: In vivo measurements taken at 20 to 40 m intervals and data points connected by straight lines.

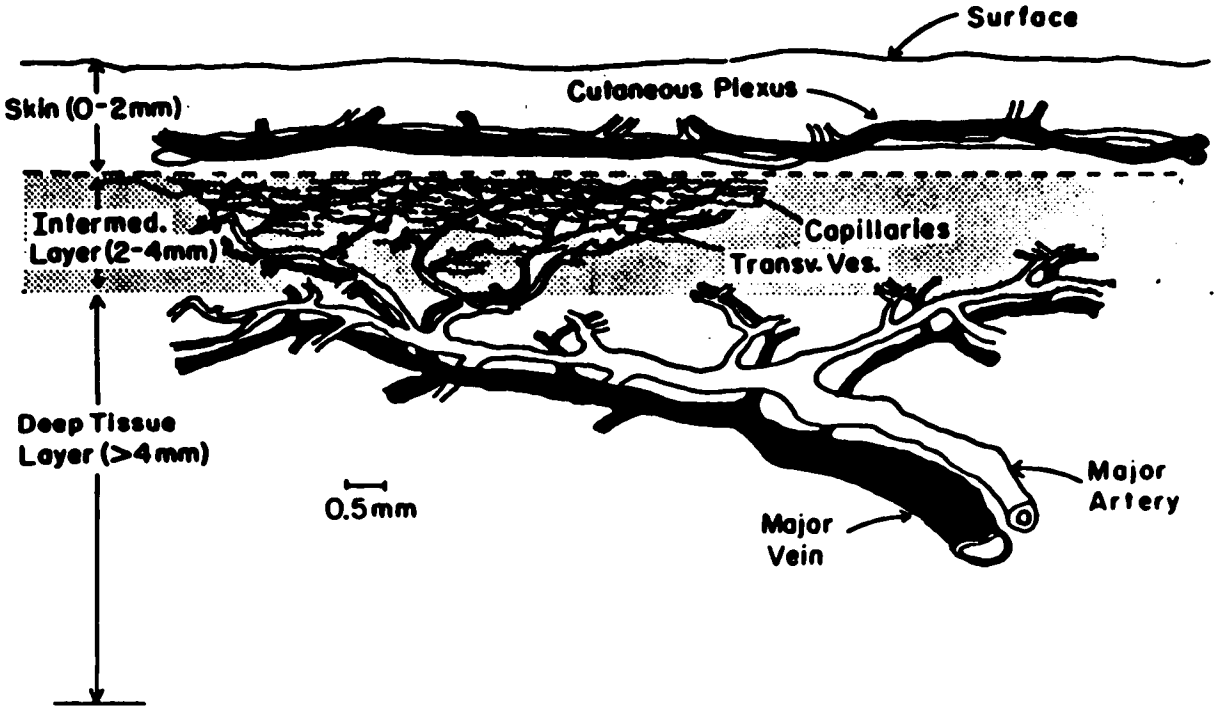

Fig. 4 Schematic of peripheral circulation

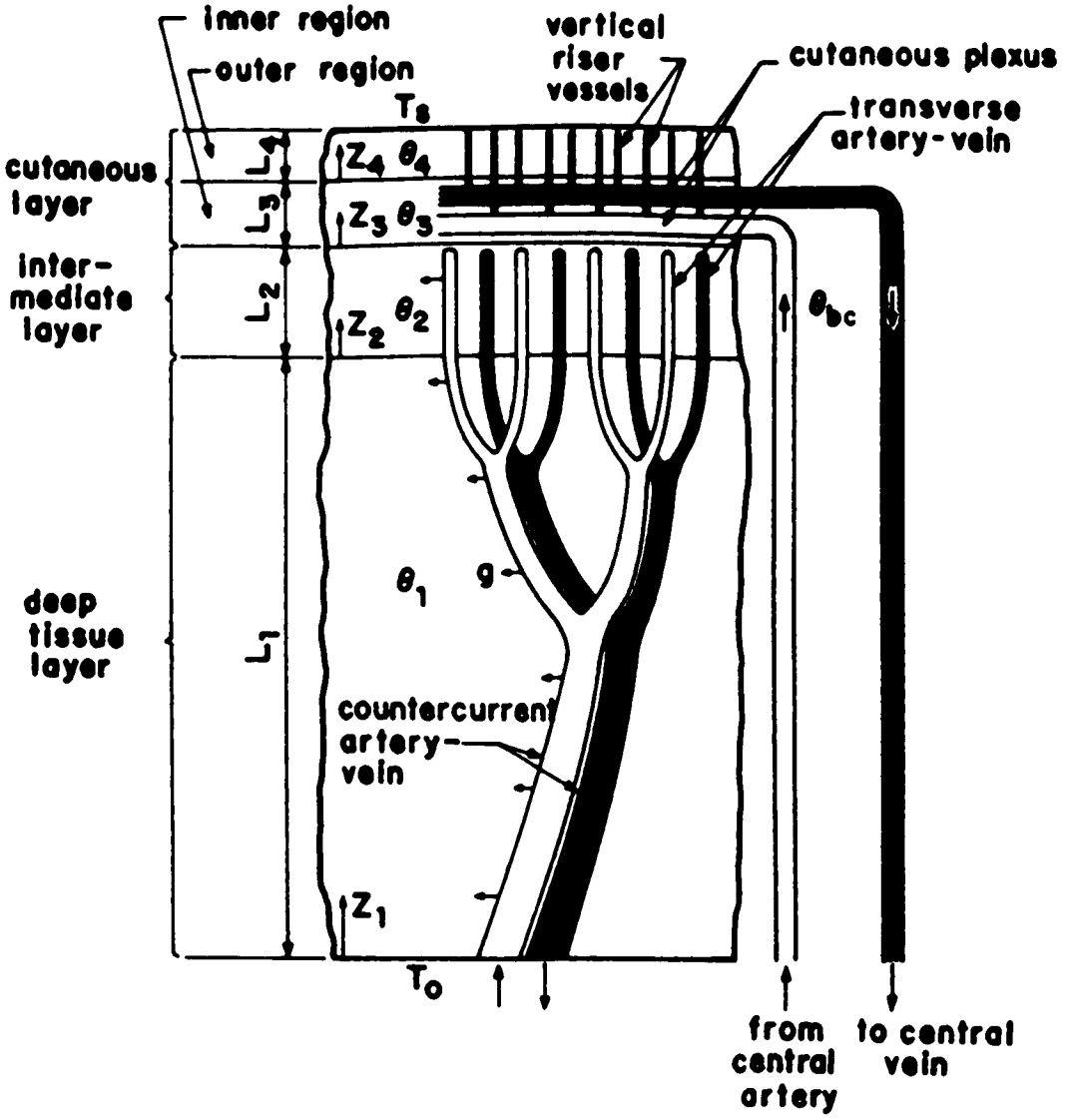

Fig.5 Simplified three-layer model showing basic vascular structure in deep, intermediate and cutaneous layers. Only thermally significant countercurrent vessels shown in region L_1 and L_2. Capillary beds omitted throughout.

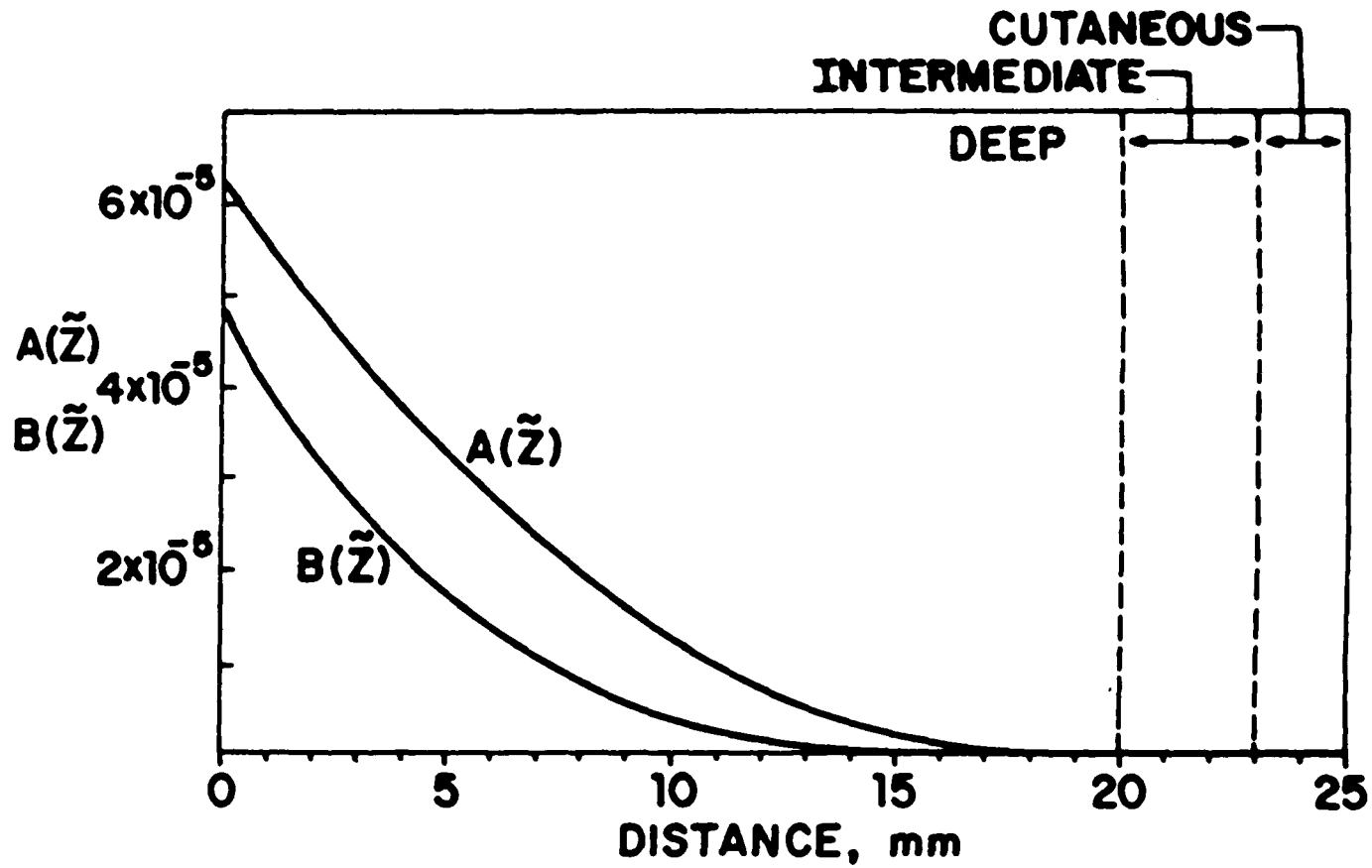

Fig.6 Functions $A(\tilde{z})$ and $B(\tilde{z})$ representing variation of vascular structure of tissue

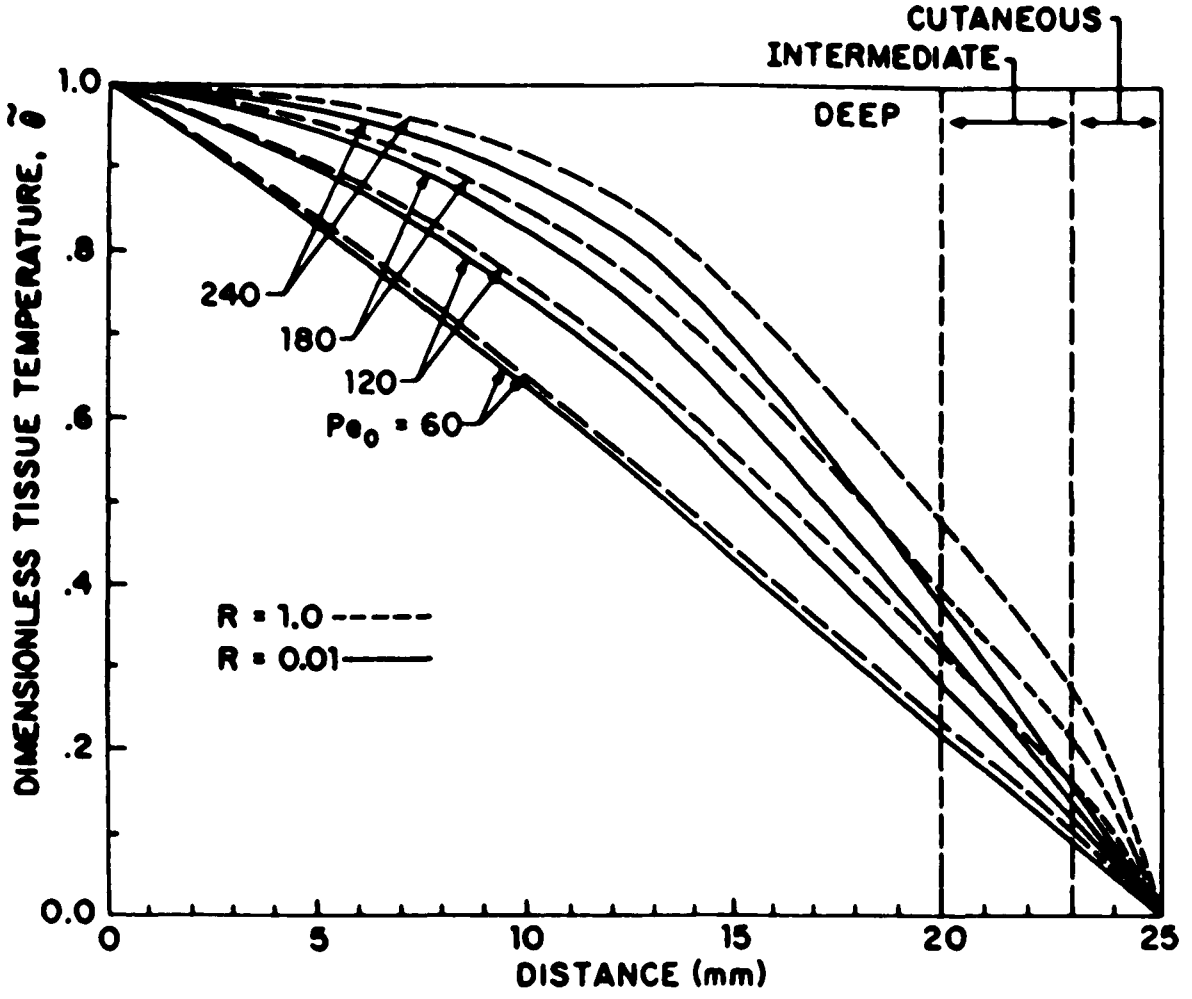

Fig.7 Effect of inflow Peclet number P_{e_0} on tissue temperature profile

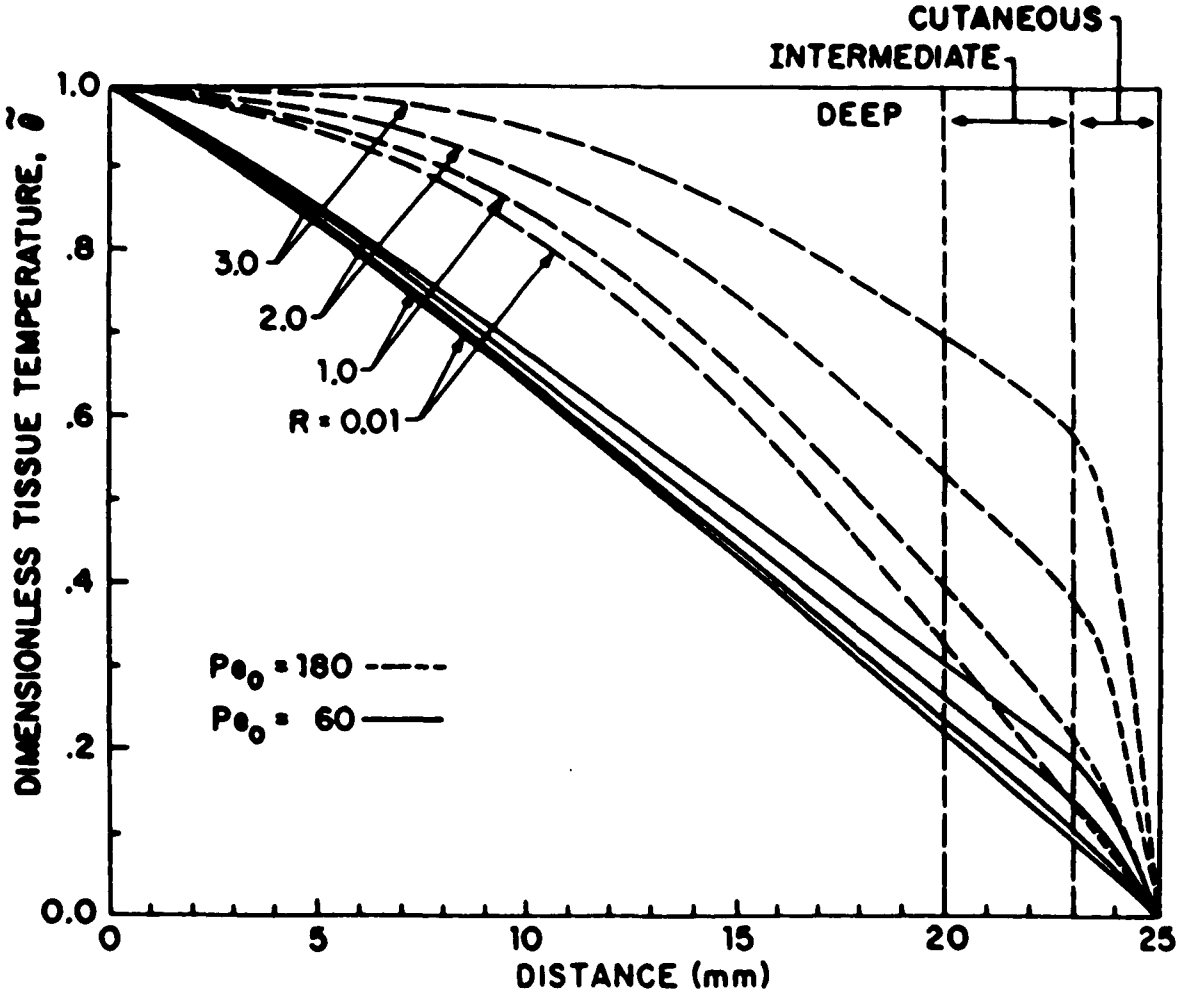

Fig.8 Effect of blood flow ratio R on tissue temperature profile

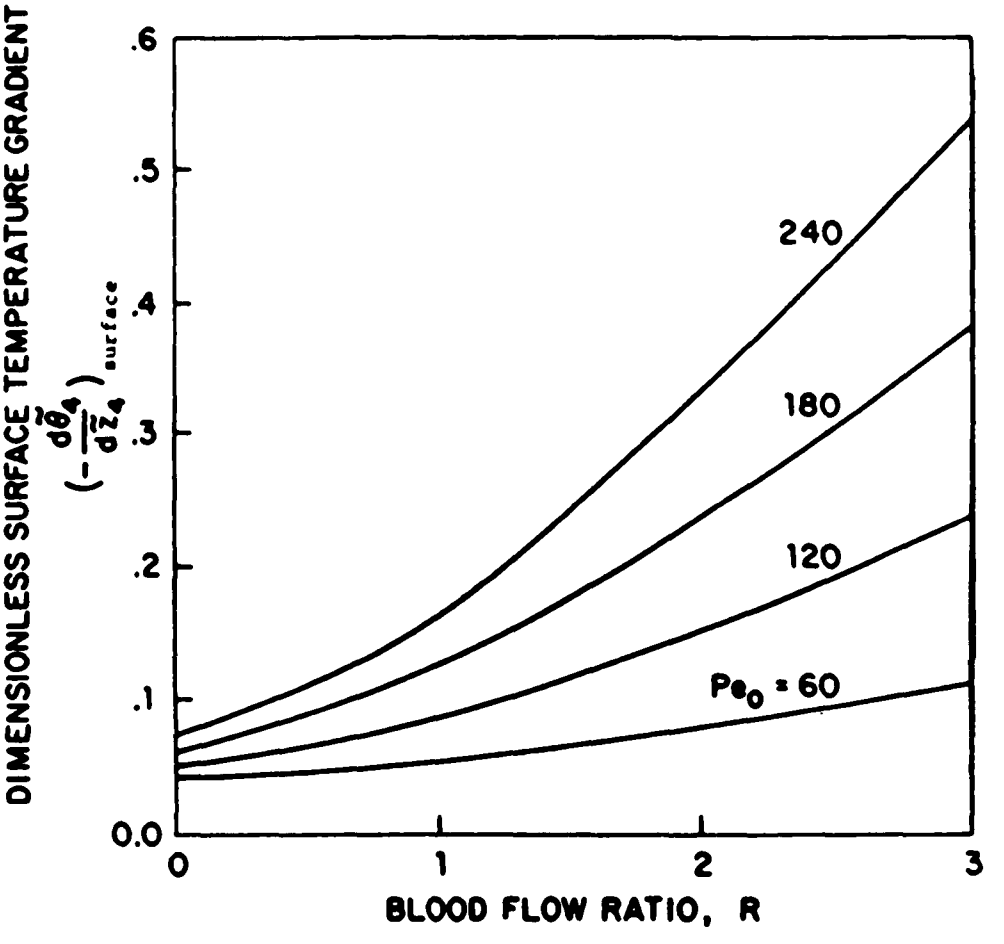

Fig.9 Effect of inflow Peclet number P_{e_0} and blood flow ratio R on surface heat flux

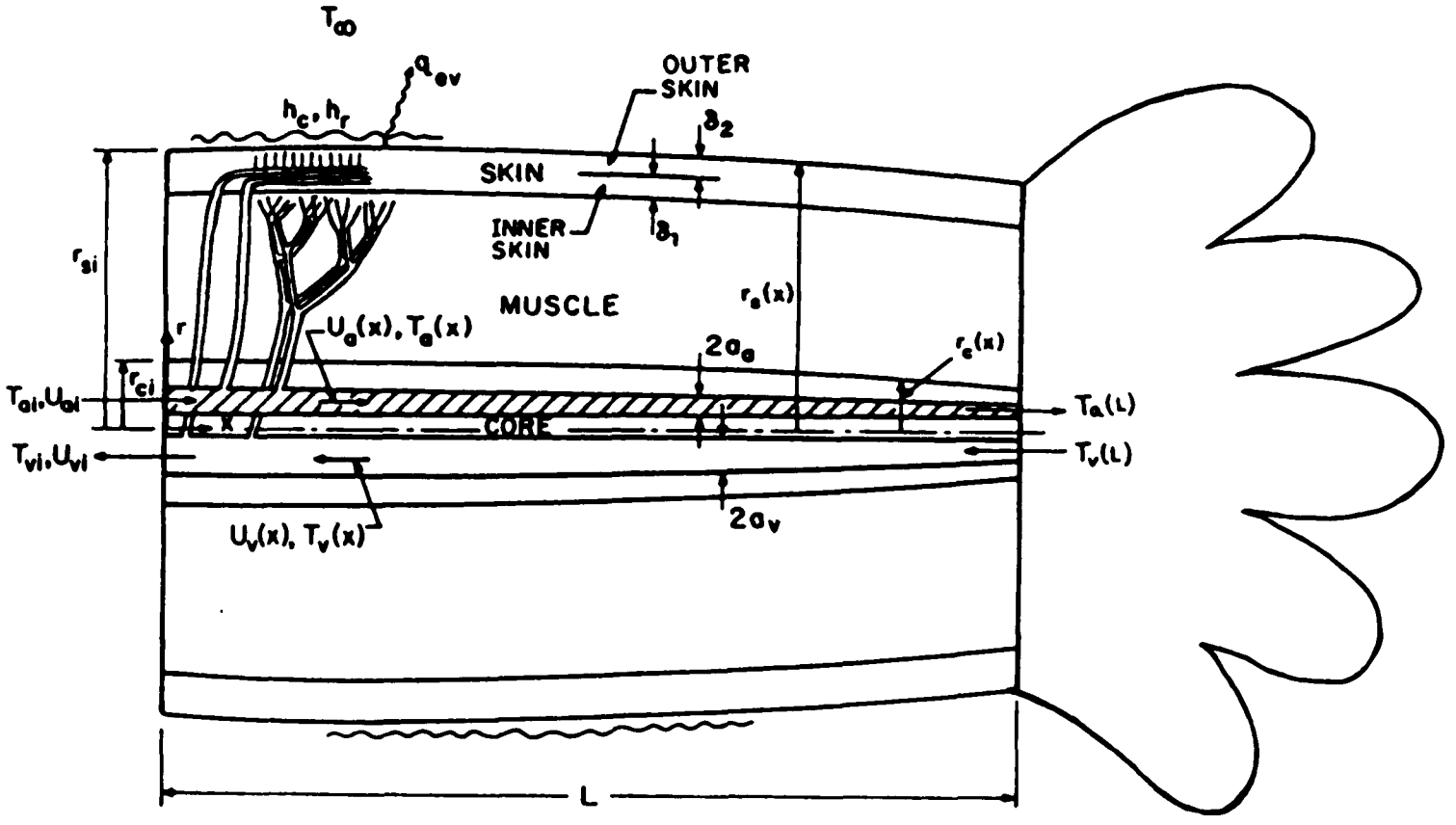

Fig.10 Schematic of entire limb model

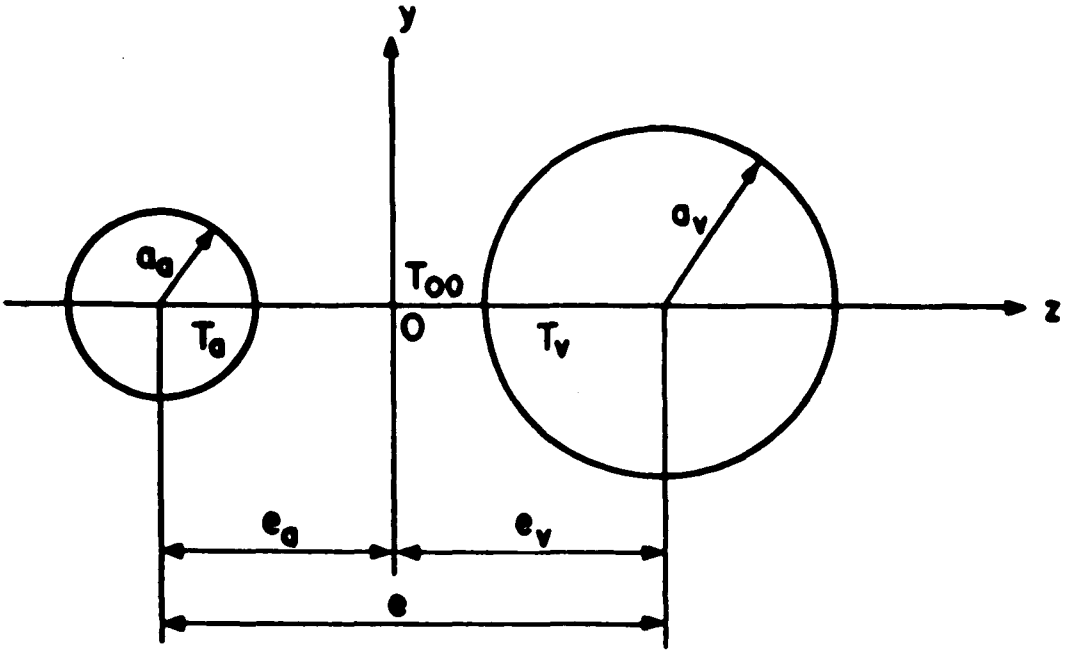

Fig.11 Schematic of countercurrent vessel pair

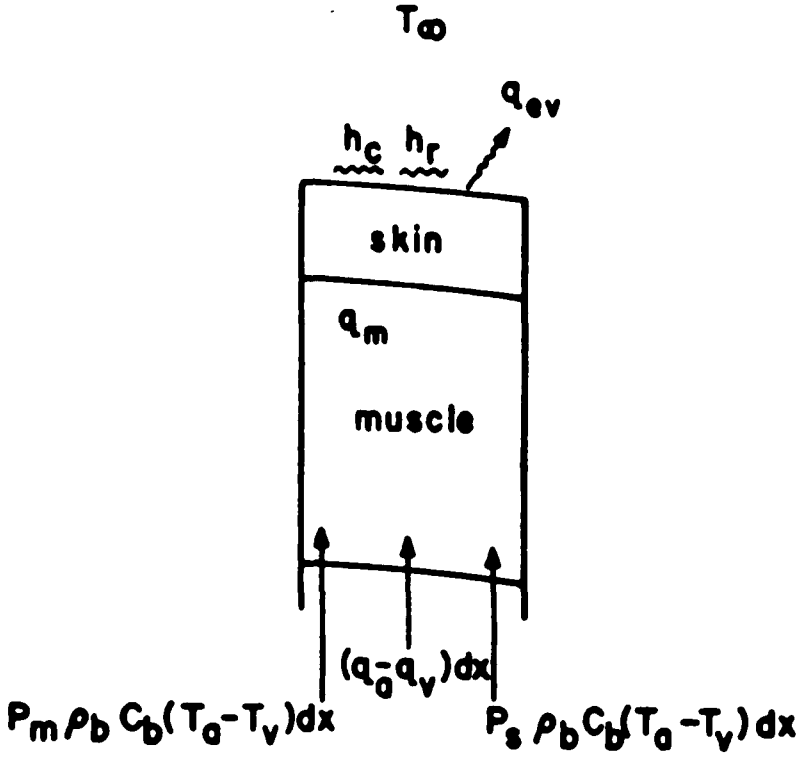

Fig.12 Heat transfer for a combined muscle-skin element

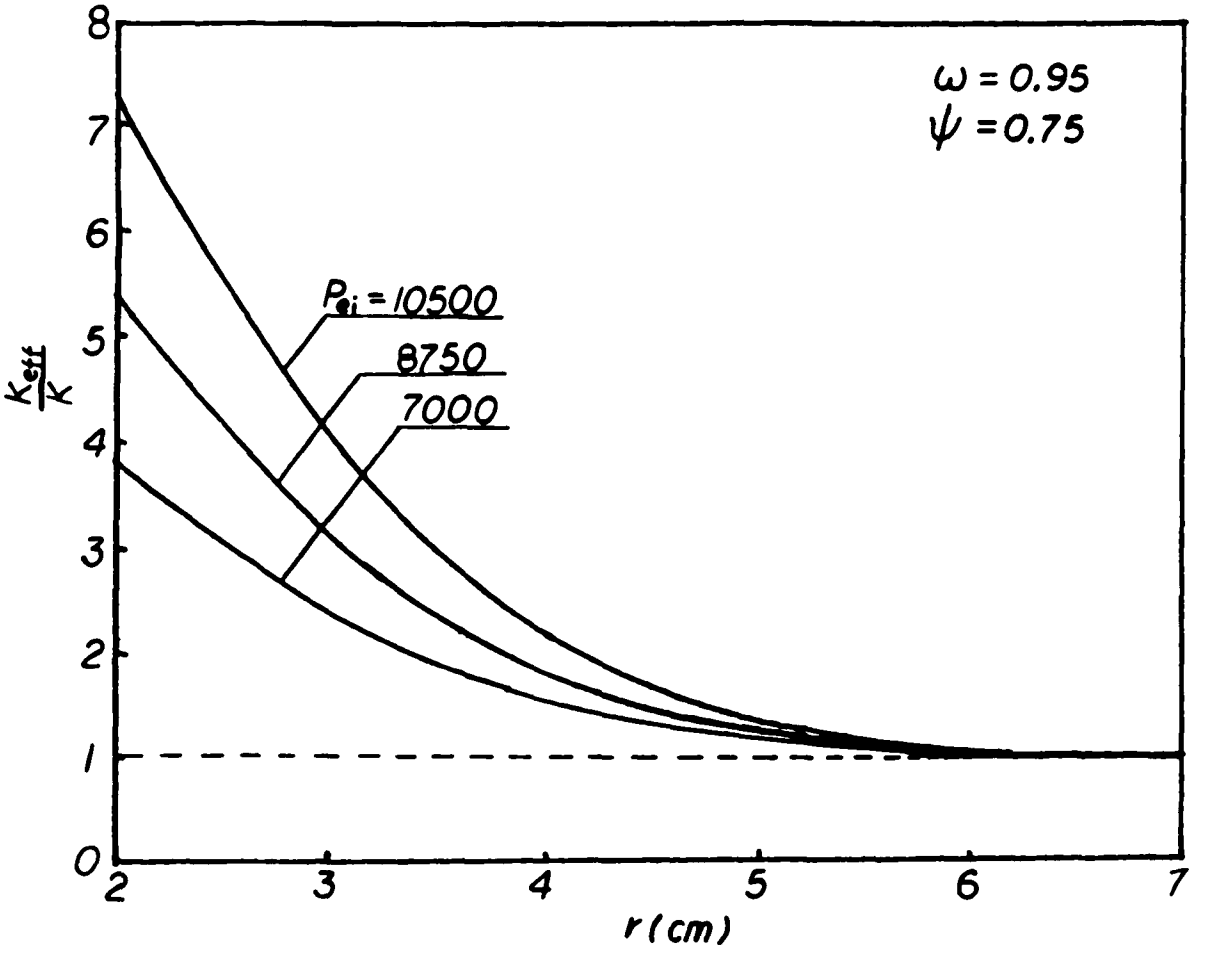

Fig.13 Variation of effective conductivity in radial direction at entrance of arm

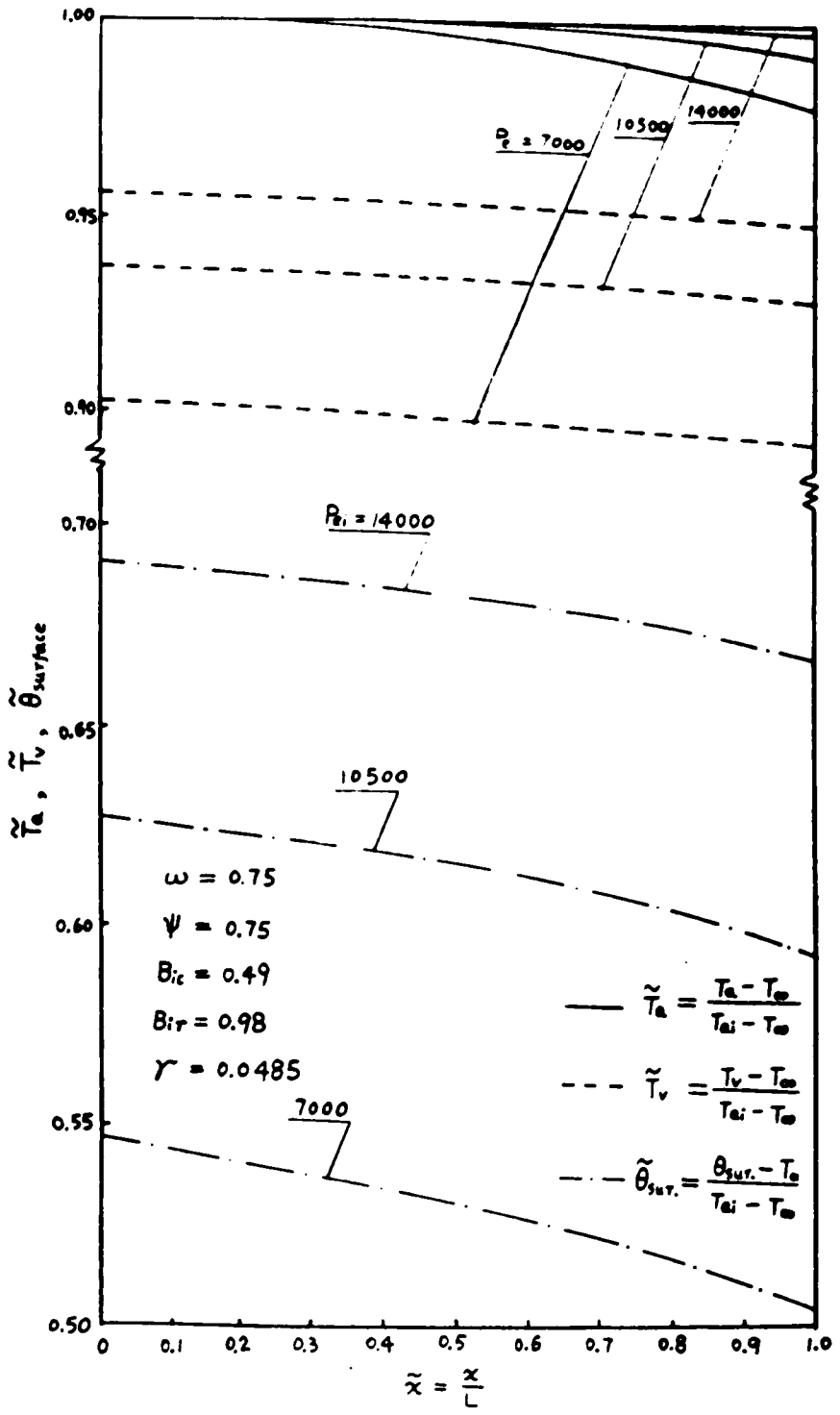

Fig.14 Effect of inflow Peclet number P_{ei} on central artery, vein and skin surface temperature profile

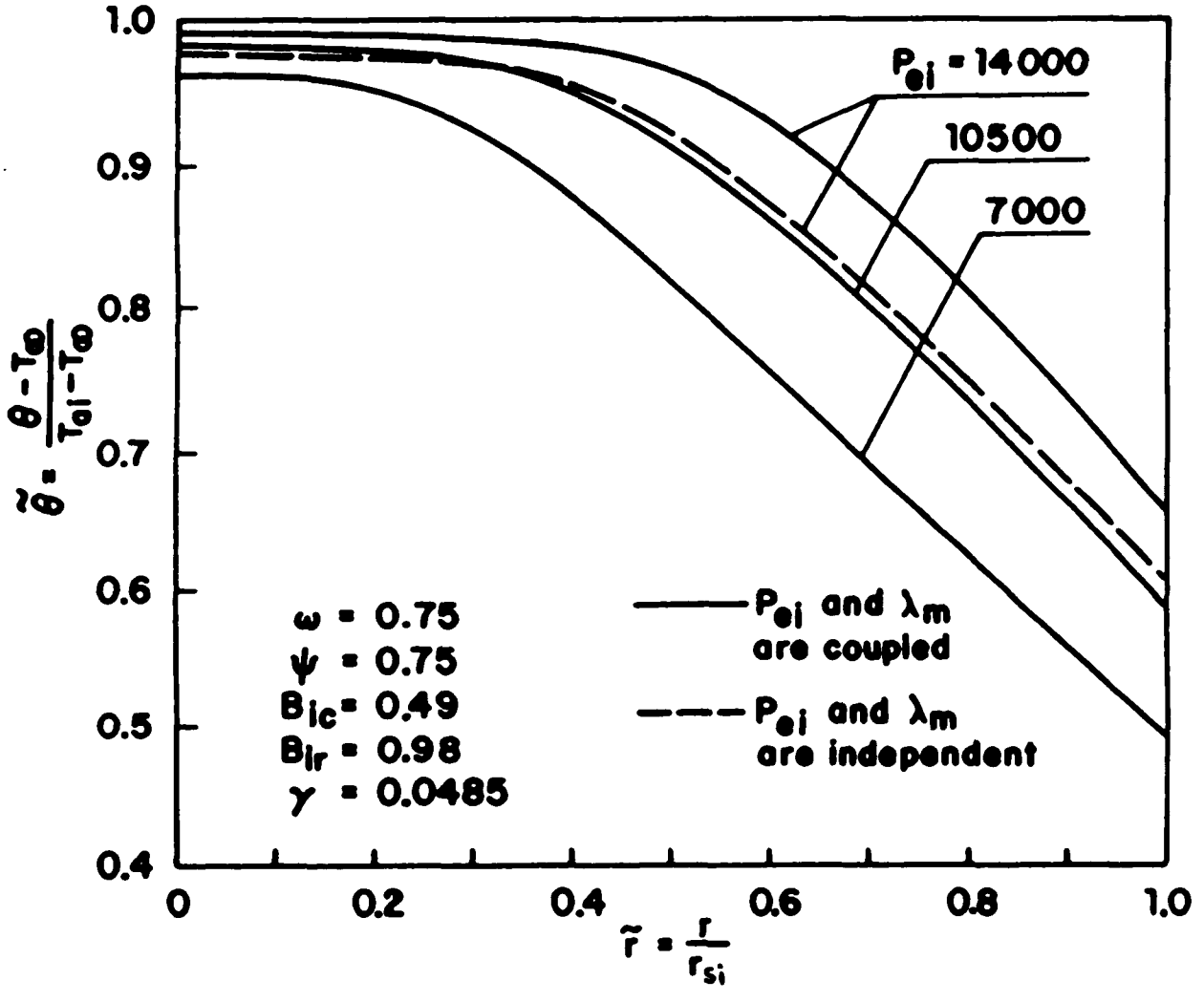

Fig.15 Effect of inflow Peclet number P_{ei} on radial temperature profile of tissue

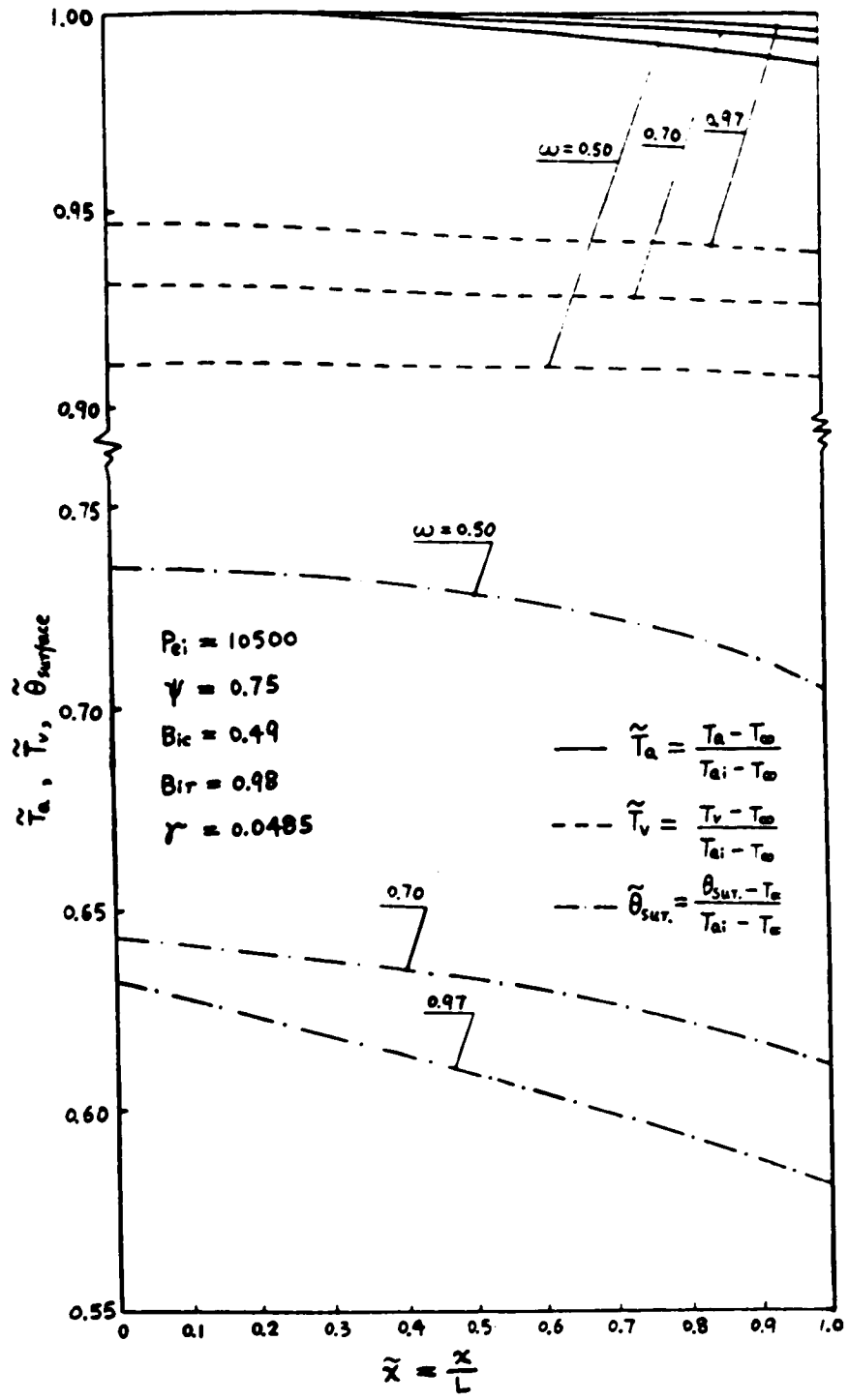

Fig.16 Effect of blood flow ratio ω on central artery, vein and skin surface temperature profile

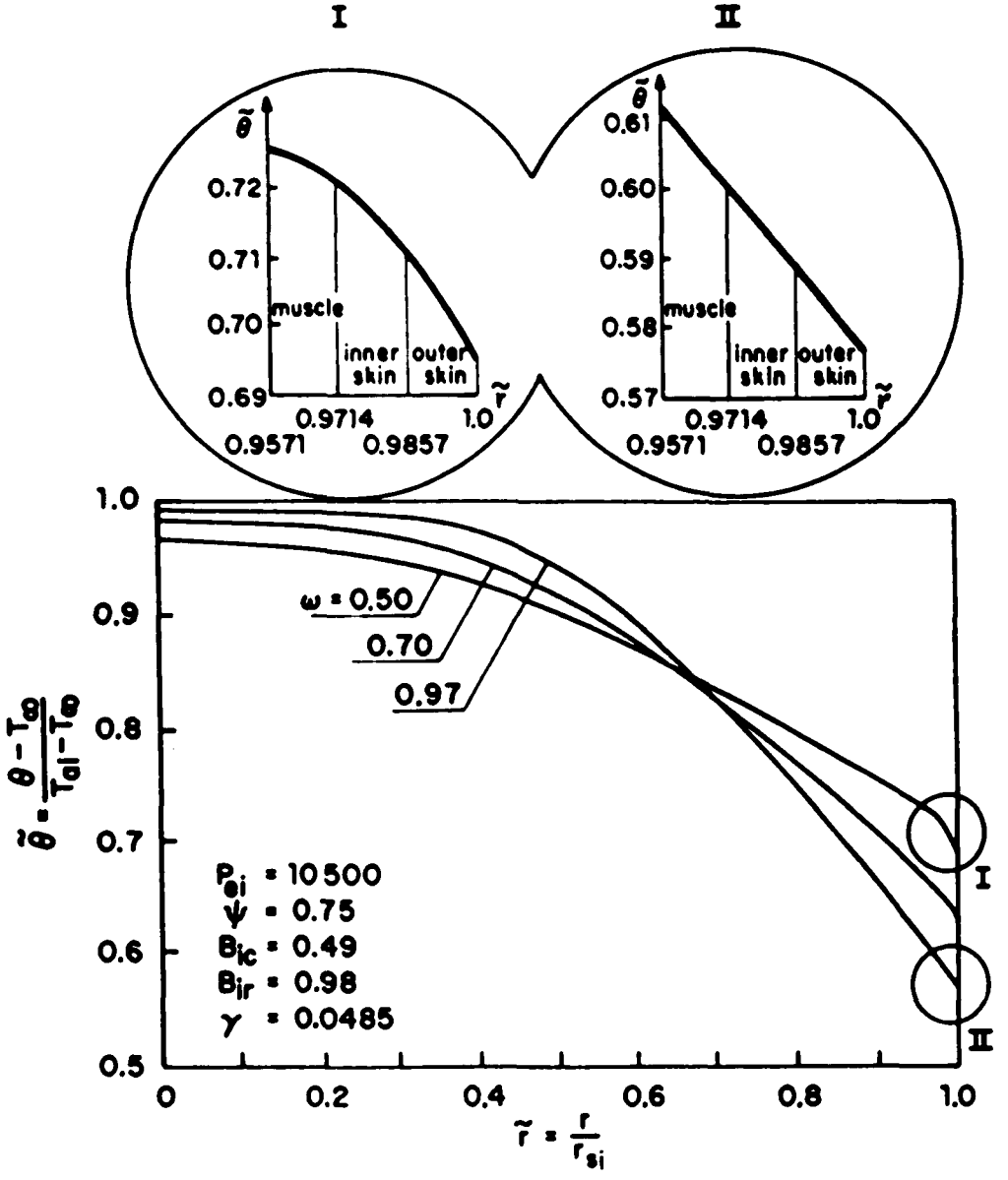

Fig.17 Effect of blood flow ratio ω on radial temperature profile of tissue

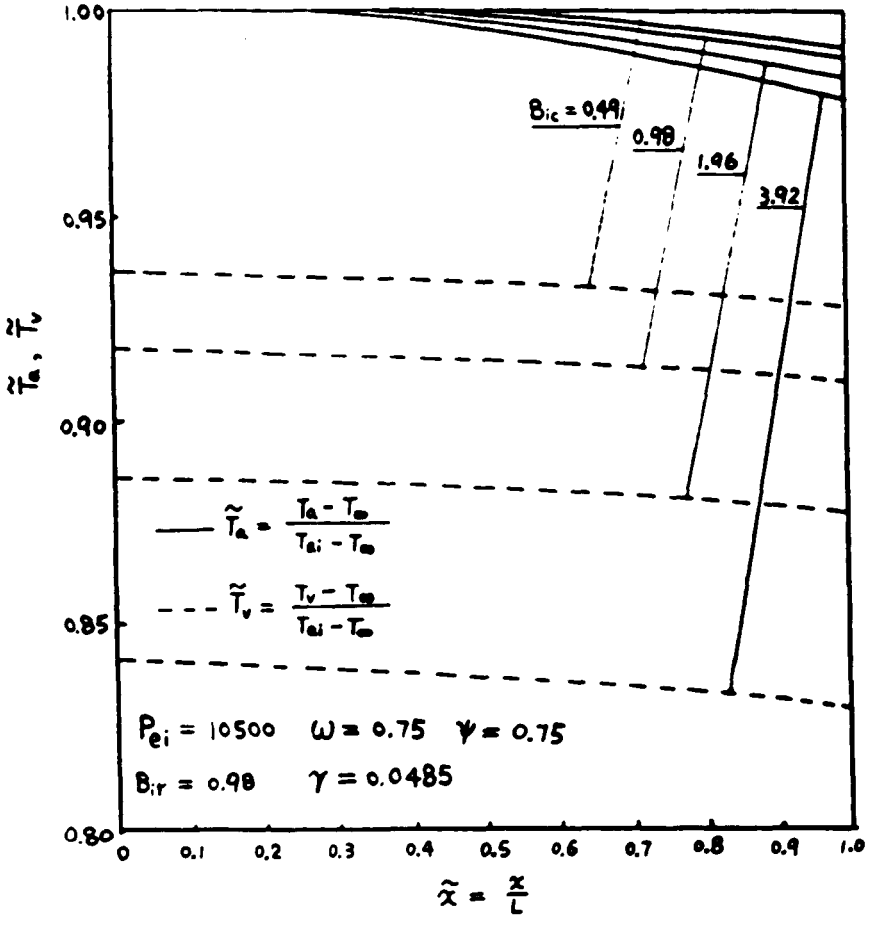

Fig. 18 Effect of convective Biot number B_{ic} on central artery and vein temperature profile

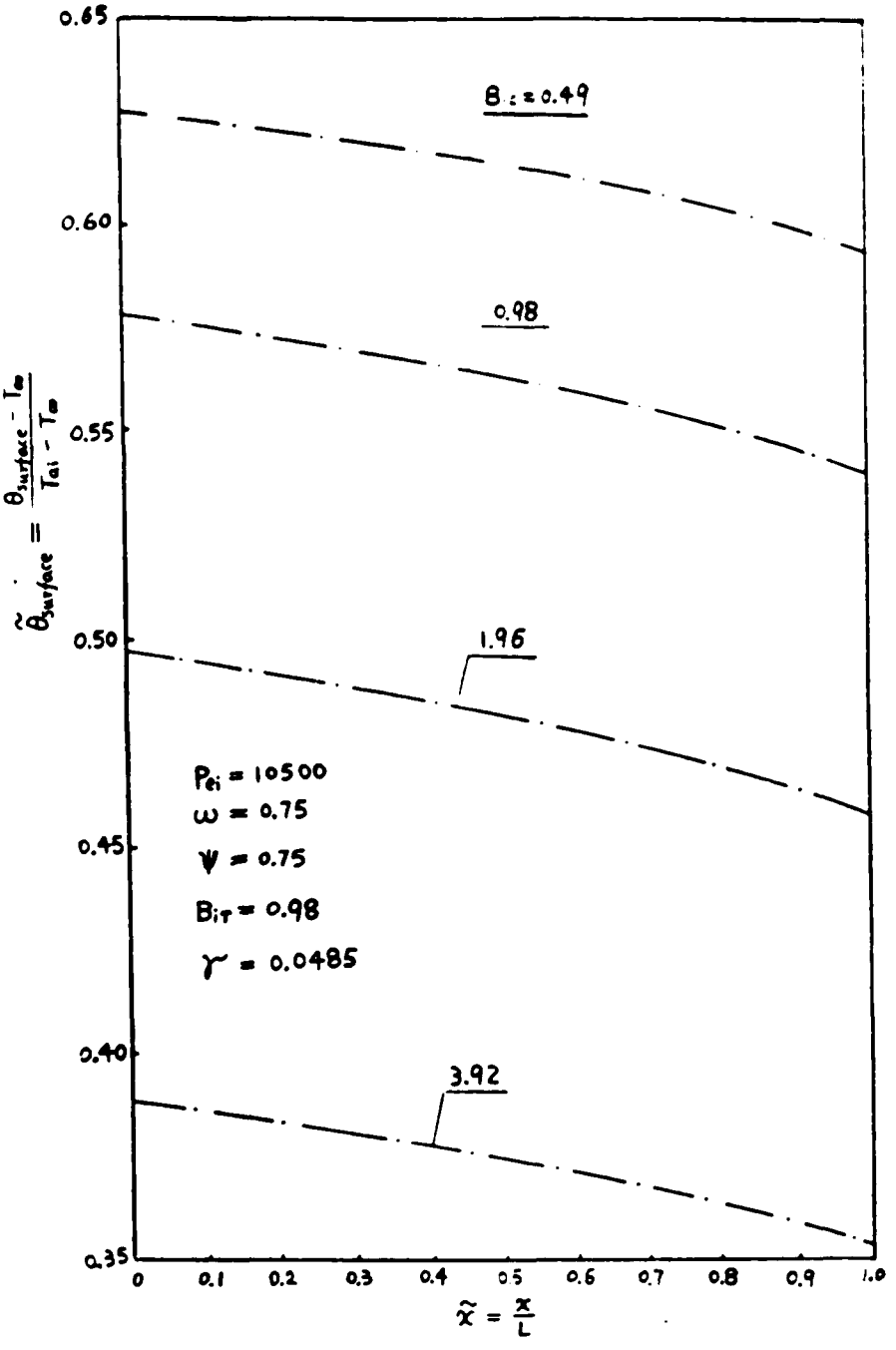

Fig.19 Effect of convective Biot number B_{ic} on skin surface temperature profile

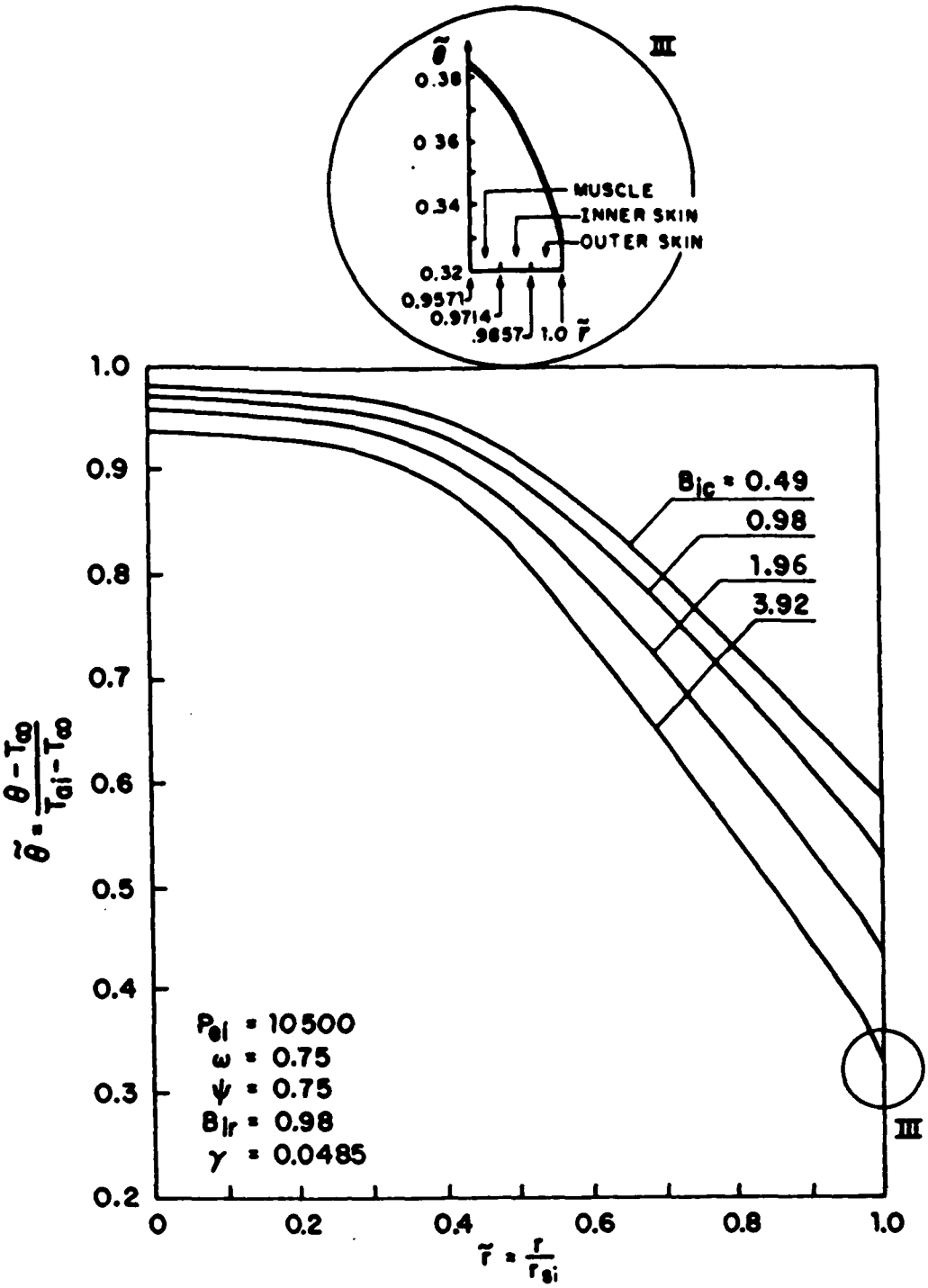

Fig. 20 Effect of convective Biot number B_{ic} on radial temperature profile of tissue

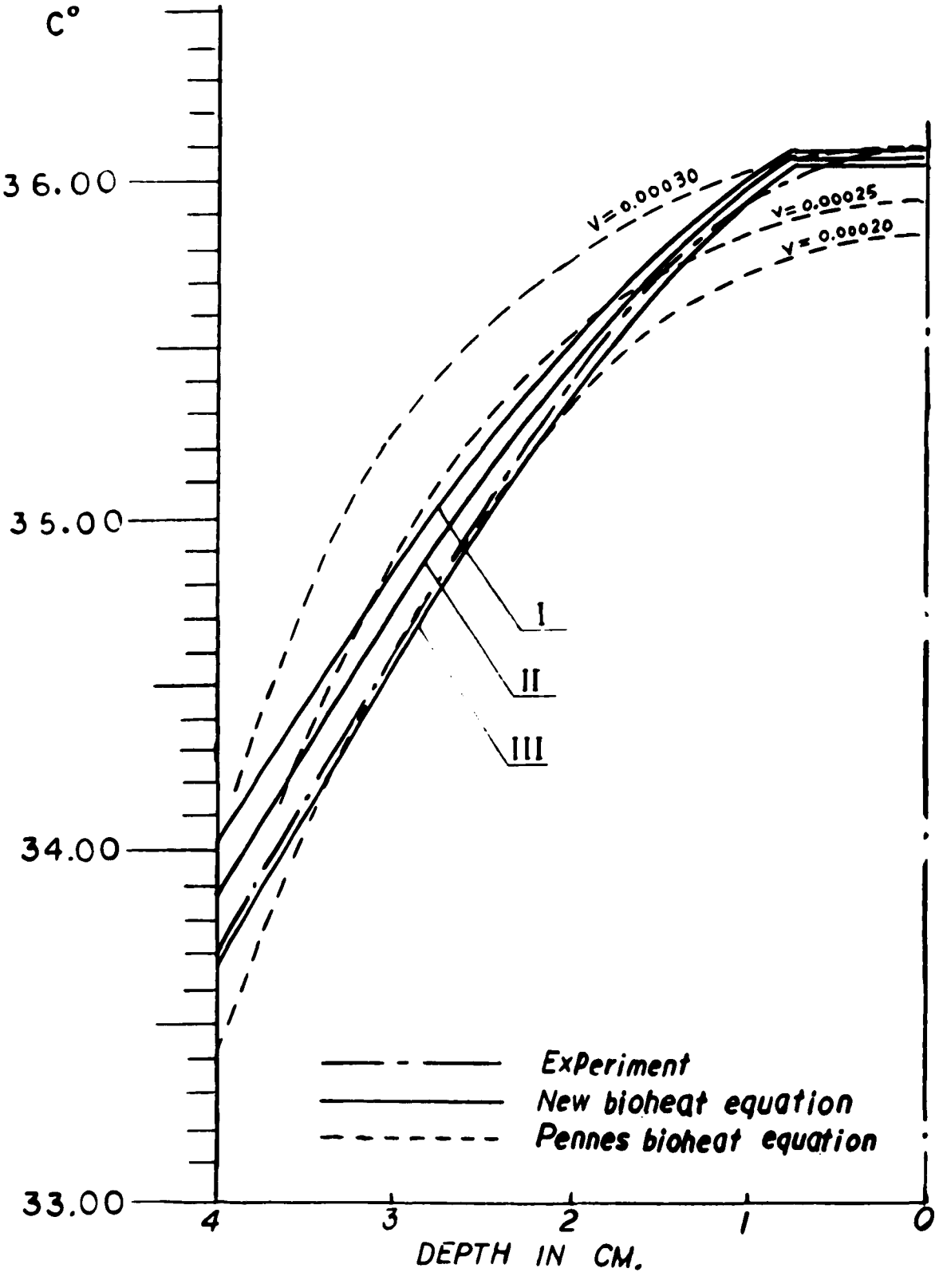

Fig.21 Comparison between theoretical predictions and experimental measurements

BIBLIOGRAPHY

1. Pennes, H. H., " Analysis of Tissue and Arterial Blood Temperatures in the Resting Forearm," Journal of Applied Physiology, Vol.1, 1948, pp.93-122.

2. Shitzer, A. and R. C. Eberhart, Ed., Heat Transfer in Medicine and Biology, Vol.1, Plenum Press, New York, 1985.

3. Wulff, W., " The Energe Conservation Equation for Living Tissue," ISEE Trans. BME-21, No.6, 1974, pp.494-495.

4. Klinger, H. G., " The Description of Heat Transfer in Biological Tissue, " Proceedings Conference on Thermal Characteristics of Tumors: Applications in Detection and Treatment, New York Academy of Science (Mar. 14-16, 1979).

5. Chen, M. M. and K. R. Holmes, " Microvascular Contributions in Tissue Heat Transfer," Annals of the New York Academy of Science, Vol.355, 1980, pp.137-150.

6. Chato, J., "Heat Transfer to Blood Vessels" ASME Journal of Biomechanical Engineering, Vol.102, 1980, pp.110-118.

7. Weinbaum, S., L. M. Jiji and D. E. Lemons, " Theory and Experiment for the Effect of Vascular Microstructure on Surface Tissue Heat Transfer. Part I: Anatomical Foundation and Model Conceptualization, " ASME Journal of Biomechanical Engineering, Vol.106, 1984, pp.321-330.

8. Jiji, L. M., S. Weinbaum and D. E. Lemons, " Theory and Experiment for the Effect of Vascular Microstructure on Surface Tissue Heat Transfer. Part II: Model Formulation and solution," ASME Journal of Biomechanical Engineering, Vol.106, 1984, pp.331-341.

9. Dagan, Z., S. Weinbaum and L. M. Jiji, " Parametric Studies on the Three Layer Microcirculatory Model for Surface Energy Exchange, " ASME Journal of Biomechanical Engineering, Vol.108, 1986, pp.89-96.

10. Weinbaum, S. and L. M. Jiji, " A New Simplified Bioheat Equation for the Effect of Blood Flow on Local Average Tissue Temperature, " ASME Journal of Biomechanical Engineering, Vol.107, 1985, pp.131-139.

11. Lemons, D. E., S. Weinbaum and L. M. Jiji, "Experimental Studies on the Role of the Micro and Macro Vascular System in Tissue Heat Transfer, " American Journal of Physiology, in Press (1987).

12. Zhu, M., D. E. Lemons, S. Weinbaum and L. M. Jiji, " On the Experimental Verification of the New Bioheat Equation of Weinbaum and Jiji and Its Extension to Microvessels of Unequal Size," Submitted to ASME Journal of Biomechanical Engineering, June,1986.

13. Bligh, J., "Regulation of Body Temperature in Men and Other Mammals," in Heat Transfer in Medicine and Biology, Eds. Shitzer, A. and R. Eberhart, Vol.1, pp.15-51, Plenum Press, New York, 1985.

14. Rowell, L. B. and C. R. Wyss, " Temperature Regulation and Heat-Stressed Man," in Heat Transfer in Medicine and Biology, Eds. Shitzer, A. and R. Eberhart, Vol.1, pp.53-78, Plenum Press, New York, 1985.

15. Hammel, H. T., "Regulation of Internal Body Temperature," Annual Review of Physiology, Vol.30, 1968, pp.641-719.

16. Huckaba, C. E., J. A. Downey and R. C. Darling, " A Feedforward-Feedback Mechanism for Human Thermoregulation, " Chemical Engineering Symposium Series, Vol.67, 1971, pp.1-7.

17. Arkin, H. and A. Shitzer, " A Model of Thermoregulation in the Human Body, " ASME Winter Annual Meeting, ASME Paper 84-WA/HT-66, 1984.

18. Sekins, K. M. and A. F. Emerby, " Thermal Science for Physical Medicine, " in Therapeutic Heat and Cold, Ed. Lehmann, J. F. Williams and Wilkings Press.

19. Fung, Y. C., " Biomechanics: A Survey of the Blood Flow Problem, " in Advances in Applied Mechanics, Eds. Yip, C. S., Vol.11, 1971, pp.65.

20. Johnson, J. M., L. B. Rowell and G. L. Brengelmann, "Modification of the Skin Blood Flow-Body Temperature Relationship by Upright Exercise, " Journal of Applied Physiology, Vol.37, 1974, pp.880-886.

21. Keller, K. H. and L. Seiler, Jr., " An Analysis of Peripheral Heat Transfer in Man, " Journal of Applied Physiology, Vol.30, 1971, pp.779-786.

22. Mitchell, J. W. and G. E. Myers, " An Analytical Model of the Countercurrent Heat Exchange Phenomena, " Biophysical Journal, Vol.8, 1968, pp.897-911.

23. Wissler, E. H., " A Mathematical Model of the Human Thermal System, " Bull. of Mathematical Biophysics, Vol.26, 1964, pp.147-166.

24. Cooney, D. O., Biomedical Engineering Principles, Vol.2, pp.104-107, Dekker, New York, 1976.

25. Song, W. J., S. Weinbaum, L. M. Jiji and D. E. Lemons, " A Variable Geometry Microvascular Model for Whole Limb Heat Transfer," Presented at the 1986 ASME Winter Annual Meeting, Anaheim.

26. Raman, E. R. and V. J. Vanhuyse, " Displacement Plethsmograph Allowing Heat Loss Measurements of Extremities," Medical and Biological Engineering, May 1975, pp.422-424.

27. Raman, E. R. and V. J. Vanhuyse, " Temperature Dependence of the Circulation Pattern in the Upper Extremities," Journal of Physiologe, Vol.249, 1975,pp.197-210.

28. Raman, E. R. and V. J. Vanhuyse, " Analytical Model for the Temperature Dependence of the Circulation Pattern in Upper Extremities," Rad. and Environm. Biophys., Vol.12, 1975, pp. 257-269.